Food Hydrocolloids 138 (2023) 108446

Contents lists available at ScienceDirect

Food Hydrocolloids

journal homepage: www.elsevier.com/locate/foodhyd

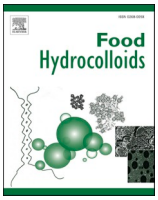

The structure and dynamics of locust bean gum in aqueous solution

Adam O'Connell [a], Francisco M. Goycoolea [b], Alessandro Gulotta [c], Peter Holmqvist [c], Peter Schuetz [d], Johan Mattsson [a,*]

[a] School of Physics and Astronomy, University of Leeds, Leeds, LS2 9JT, United Kingdom
[b] School of Food Science and Nutrition, University of Leeds, Leeds, LS2 9JT, United Kingdom
[c] Lund University, Division of Physical Chemistry, Lund, Sweden
[d] Unilever R&D, Colworth, MK44 1LQ, United Kingdom

ARTICLE INFO

Keywords:
Locust bean gum
Galactomannans
Viscosity
Structure
Light scattering

ABSTRACT

Locust bean gum (LBG) is an industrially important polysaccharide used widely in food, cosmetics, textiles, and biopharmaceutical applications, where understanding its solution behaviour is important for formulation design. To address this, we investigate the structure and dynamics of LBG in aqueous solution using steady state shear rheology, static light scattering (SLS), ultra-small-angle light scattering (USALS), and dynamic light scattering (DLS). We find that steady state shear rheology mainly probes the well-dispersed LBG fraction, whereas the scattering response is dominated by supramolecular LBG aggregates. We identify three viscosity-concentration regimes (dilute, semidilute unentangled, and semidilute entangled), with scaling behaviour largely consistent with predictions for neutral flexible polymers. SLS and USALS provide evidence for the existence of two separate populations of aggregated structures, where SLS mainly probes the internal structure of the smaller aggregate population. The solution dynamics are dominated by a 'slow' decay mode, which is consistent with Zimm dynamics and attributed to relaxations within the aggregates. In dilute solutions, the apparent viscosity associated with this mode is greater than the solution viscosity, but the two converge as concentration is increased. An additional 'fast' mode is observed within the semidilute range, associated with the dispersed polymer fraction, and attributed to cooperative diffusion. Our study provides comprehensive insight into the structure and dynamics of aqueous LBG solutions—paving the way for a greater fundamental understanding of galactomannans in solution, and for increased control over LBG-based formulations of industrial interest.

1. Introduction

Locust bean gum (LBG) is a polysaccharide produced from the seeds of the carob tree, *Ceratonia siliqua*, used widely in the food industry due to its strong thickening properties and natural origins (Saha & Bhattacharya, 2010). Other uses include cosmetic, paper, and textile products (Barak & Mudgil, 2014), as well as an increasing number of niche applications, for example in biopharmacy (Grenha & Dionísio, 2012; Perestrelo, Grenha, Rosa Da Costa, & António Belo, 2014; Ventura, Paninho, Nunes, Fonseca, & Branco, 2015), nanoparticle synthesis (Maiti et al., 2010; Tagad et al., 2014), edible food coatings (Cerqueira et al., 2011; Parafati, Vitale, Restuccia, & Cirvilleri, 2016), and as a bio-electrolyte in zinc-ion batteries (Liu et al., 2021).

LBG belongs to the family of galactomannans, and is composed of a linear backbone of β-D-mannose units, connected by 1,4-linkages, and α-D-galactose side-groups, connected by 1,6-glycosidic linkages (Fig. 1a) (Pegg, 2012). The ratio of mannose to galactose units (M:G) for LBG is often given as ~ 4:1 (Goff, Ferdinando, & Schorsch, 1999; Richardson & Norton, 1998; Tanaka, Hatakeyama, & Hatakeyama, 1998a), although this varies due to source, growing conditions, solution preparation, and characterisation method. Indeed, published measurements can be found in a range as wide as 2.8–4.2 (Andrade, Azero, Luciano, & Gonçalves, 1999; Daas, Schols, & De Jongh, 2000; Dakia, Blecker, Robert, Wathelet, & Paquot, 2008; Launay, Cuvelier, & Martinez-Reyes, 1997; Lopes da Silva & Goncalves, 1990; McCleary, Clark, Dea, & Rees, 1985; Richardson & Norton, 1998; Sittikijyothin, Torres, & Gonçalves, 2005). This is a relatively low degree of galactose content in comparison with other galactomannans used commonly in industry, such as guar gum (M:G ~ 2:1) and tara gum (M:G ~ 3:1) (Tanaka et al., 1998a). The molecular weight of LBG also varies with growing and processing conditions, but is typically reported to be ~ 300–2000 kDa, corresponding to a backbone degree of polymerisation of ~ 1300–9000 mannose units

* Corresponding author.
E-mail address: k.j.l.mattsson@leeds.ac.uk (J. Mattsson).

https://doi.org/10.1016/j.foodhyd.2022.108446
Received 12 September 2022; Received in revised form 5 December 2022; Accepted 28 December 2022
Available online 4 January 2023

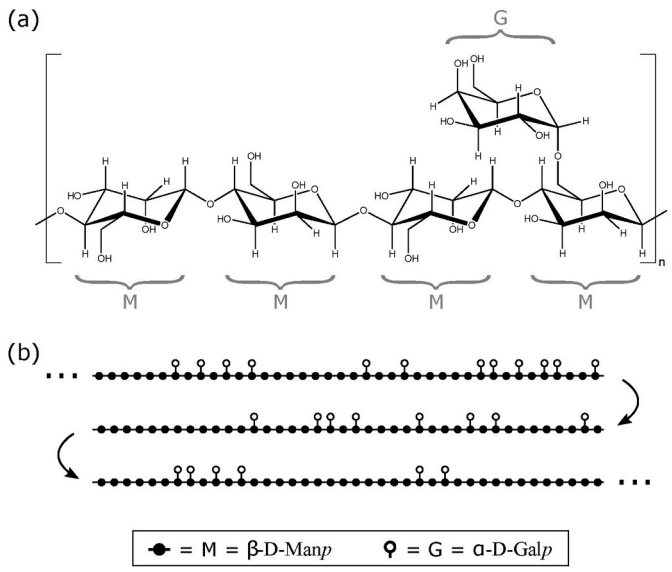

Fig. 1. The chemical structure of LBG. (a) A representative section of the mannose backbone with a single galactose side unit. (b) A larger section of an LBG molecule illustrating the distribution of galactose residues; the galactose content of this section is 18%.

(assuming M:G = 4:1) (Barak & Mudgil, 2014).

The number and distribution of galactose substituents in galactomannans strongly influence their properties, as the mannose backbone is essentially insoluble in water, while the galactose side units increase solubility (Doyle, Lyons, & Morris, 2009; Picout, Ross-Murphy, Errington, & Harding, 2001). Due to the difference in galactose content, LBG (M:G ~ 4:1) is generally less soluble in water than for example guar gum (M:G ~ 2:1) and thus typically requires treatment at higher temperatures for maximum dissolution. In a given sample of LBG, molecular variation in galactose content and distribution leads to polydispersity in solubility, allowing for fractionation by variation of temperature (Gaisford, Harding, Mitchell, & Bradley, 1986; Lopes da Silva & Goncalves, 1990). Solubility studies have observed increasing M:G ratios in sample fractions prepared at higher dissolution temperatures, and it has been demonstrated that treatment at $\gtrsim 80$ °C is required for maximum dissolution (Gaisford et al., 1986; Lopes da Silva & Goncalves, 1990). The pattern of galactose substitution is also known to influence chain conformation, flexibility, and other properties such as the interactions with xanthan gum (Dea, Clark, & McCleary, 1986; Petkowicz, Reicher, & Mazeau, 1998).

The galactose distribution in LBG has been studied through analysis of the oligomers produced by enzymatic hydrolysis (Daas et al., 2000; McCleary et al., 1985). In one of these studies, the distribution was found to be more block-like than random for all LBG sources, with a greater number of substituted couplets and long unsubstituted backbone regions than expected for a random distribution (McCleary et al., 1985). Fig. 1b illustrates a section of an LBG molecule, which we created by chain extension using a second nearest-neighbour Markov chain process based on these results. However, a similar study, which included a wider range of galactomannans, found either more block-like or more evenly-spaced distributions for LBG, depending on the source (Daas et al., 2000); thus, the results of such studies have been somewhat inconclusive.

LBG exhibits interesting phase behaviour in solution, such as cryogelation (Goff et al., 1999; Patmore, Goff, & Fernandes, 2003; Tanaka et al., 1998a; Tanaka, Hatakeyama, & Hatakeyama, 1998b), weak gelation upon long-term storage (Dea et al., 1977; Garnier, Schorsch, & Doublier, 1995), and phase separation in the presence of milk proteins (Patmore et al., 2003; Schorsch, Jones, & Norton, 1999). Associations between galactose-poor backbone regions have been suggested as the mechanism for gelation (Dea et al., 1986), and have also been used to explain the strong thickening behaviour in solution (in which context they have been termed 'hyperentanglements') (Morris, Cutler, Ross-Murphy, Rees, & Price, 1981). It has been suggested that unsubstituted regions of six or more adjacent mannose units are required for these associations, and thus that 'blockier' galactose distributions will lead to greater levels of association than random distributions, as the latter will have fewer stretches of unsubstituted backbone segments (Dea et al., 1986). Experimentally, it has been observed that galactomannan gelation requires a sufficiently low degree of galactose substitution (Dea et al., 1977; Tanaka et al., 1998a), but studies on the viscosity scaling of highly substituted galactomannans (M:G ~ 1:1) have reached conflicting conclusions on the nature of proposed 'hyperentanglements', and indeed whether such an interaction is necessary to explain galactomannan solution viscosity behaviour (Doyle et al., 2009; Ganter, Milas, Corrêa, Reicher, & Rinaudo, 1992).

In this work, we characterised industrially relevant solutions of LBG in water using steady state shear rheology, static light scattering, ultra-small-angle light scattering, and dynamic light scattering. These techniques were found to be highly complementary, and their combined use on consistently prepared solutions allowed for a detailed understanding of LBG solution behaviour.

2. Theory and methodology background

2.1. Viscosity scaling of polymer solutions

The viscosity scaling of polymer solutions is typically characterised by the relationship between two dimensionless variables: the specific viscosity and the reduced polymer concentration. The specific viscosity characterises the relative increase in solution viscosity due to the addition of a solute, and is defined as $\eta_{sp} = (\eta_0 - \eta_s)/\eta_s$, where η_s is the solvent viscosity, and η_0 is the zero-shear viscosity, as determined by e.g. steady shear rheology or capillary viscometry. The reduced concentration is defined as $c[\eta]$, where $[\eta]$ is the intrinsic viscosity (Rubinstein & Colby, 2003), typically calculated as the zero-concentration limit of η_{sp}/c. $[\eta]$ is approximately equal to the inverse of the chain overlap concentration ($1/c^*$), and $M[\eta]$, where M is the chain molar weight, is thus a measure of the volume occupied by a single polymer coil at infinite dilution (Rubinstein & Colby, 2003). The scaling of η_{sp} with $c[\eta]$ is generally described by power laws, characterised by different scaling exponents in different concentration regimes.

For $c < c^*$, solutions are in the dilute regime. Here, molecules essentially adopt the dimensions of isolated molecules and occupy less than the full volume of the solution. Hydrodynamic interactions are important and the Zimm model predicts that the specific viscosity scales as $\eta_{sp} \sim c[\eta]$ (Colby, 2010; Rubinstein & Colby, 2003).

For $c^* < c < c^e$ (the entanglement concentration), solutions are in the semidilute unentangled regime. Here, molecules interpenetrate, leading to a change in viscosity scaling. Hydrodynamic interactions are screened by neighbouring molecules, and are no longer significant on the length-scale of entire chain relaxation. Thus, the Rouse model is used to predict the viscosity scaling, giving $\eta_{sp} \sim (c[\eta])^{1.3}$ or $\eta_{sp} \sim (c[\eta])^{2.0}$, for good and θ solvents, respectively (Colby, 2010; Rubinstein & Colby, 2003).

For $c > c^e$, solutions are in the entangled regime. The onset of molecular entanglements leads to a significantly enhanced growth of viscosity with concentration, predicted as $\eta_{sp} \sim (c[\eta])^{3.9}$ or $\eta_{sp} \sim (c[\eta])^{4.7}$, for good and θ solvents, respectively (Colby, 2010; Rubinstein & Colby, 2003). Excluded volume interactions are progressively screened by interpenetrating neighbouring molecules as concentration is increased within the semidilute regimes (Rubinstein & Colby, 2003).

The concentration-dependent polymer solution viscosity is sometimes alternatively described using a simpler approach including only two power law regimes, particularly when the semidilute unentangled regime is very narrow (Doyle et al., 2009; Dumitriu, 2004; Pollard & Fischer, 2014). We also note an alternative description based on a

hydrodynamic scaling theory (Phillies, 1995, 2011), for which the specific viscosity is expected to follow a stretched exponential form:

$$\eta_{sp} = \exp(ac^{\zeta_H}) - 1 \ , \tag{1}$$

where a is a system-dependent prefactor and the exponent ζ_H typically falls within the range 0.5–1.0 (Phillies, 1995, 2011; Potier, Tea, Benyahia, Nicolai, & Renou, 2020). This form has been demonstrated to successfully describe viscosity scaling over a broad concentration range for many polymer systems, although a transition to power law scaling at high concentrations has sometimes been invoked (Phillies, 1995).

2.2. Light scattering on polymer solutions

In light scattering experiments, the intensity of scattered light is recorded at different angles with respect to the incoming beam. The scattering angle, θ, corresponds to a scattering wavevector of magnitude:

$$q = \frac{4\pi n}{\lambda_0} \sin\left(\frac{\theta}{2}\right) \ , \tag{2}$$

where n is the sample refractive index and λ_0 is the vacuum wavelength of the used laser source. The length-scale probed is $\sim 1/\ q$; thus, a variation of θ provides a means to study length-scale-dependent behaviour.

2.2.1. Static light scattering (SLS)

The scattered intensity recorded in SLS, $I(q)$, contains contributions from the solvent as well as the solute, and is also affected by experimental factors such as the incoming laser intensity, scattering volume, detector properties etc. These factors are accounted for by conversion of $I(q)$ to the excess Rayleigh ratio, $\Delta R(q)$, using

$$\Delta R(q) = \frac{I(q) - I_s(q)}{I_{ref}(q)} \left(\frac{n}{n_{ref}}\right)^2 R_{ref} \ , \tag{3}$$

where $I_s(q)$ is the solvent scattering intensity, n is the solution refractive index, and $I_{ref}(q)$, n_{ref}, and R_{ref}, are respectively the measured scattering intensity, refractive index, and Rayleigh ratio of a reference sample (Berry & Cotts, 1999; Schärtl, 2007).

As q is varied, polymers in solution can be probed on length-scales ranging from greater than the size of individual molecules (characterised by their radius of gyration, R_g) to length-scales corresponding to their internal structure ($1/q < R_g$). The internal polymer structure is typically fractal, where the mass contained within a sphere of size L scales as $\sim L^{d_f}$, where d_f is the fractal dimension (Rubinstein & Colby, 2003). Static scattering from fractal objects typically reflects the mass scaling law, with the form $\Delta R(q) \sim q^{-d_f}$ (Teixeira, 1986).

Neutral polymers in dilute θ solvent conditions adopt a random walk conformation, characterised by $d_f = 2$. In good solvent conditions, excluded volume interactions lead to more extended conformations, characterised by $d_f \approx 1.7$. A fractal dimension greater than 2 indicates either poor solvent conditions, branching, or aggregation (Gittings et al., 2000). The expected scattering profile for dilute solutions of unbranched neutral polymers is thus a plateau of constant intensity for $q < 1/R_g$, followed by the form $\Delta R(q) \sim q^{-d_f}$ for $q > 1/R_g$. For fractal polymeric aggregates, the overall form is the same, but the crossover q-value and power law exponent correspond to $1/R_g$ and the fractal dimension of the aggregates, respectively.

In semidilute solutions, polymer scattering is determined by the static correlation length ξ_s, the length-scale on which excluded volume interactions are screened (approximately corresponding to the distance between polymer chains) (Colby, 2010; Uematsu, Svanberg, & Jacobsson, 2005). A scattering plateau is observed for length-scales above ξ_s, while the scattering at length-scales below ξ_s reflects the internal structure of the coils (de Gennes, 1979), which can change with concentration.

2.2.2. Dynamic light scattering (DLS)

In DLS, the time-dependent scattered intensity $I(t)$ is measured and the intensity autocorrelation function, $g_2(\tau)$, is determined as a function of lag time (τ):

$$g_2(q,\tau) = \frac{\langle I(t)I(t+\tau)\rangle}{\langle I(t)\rangle^2} \ . \tag{4}$$

In the Gaussian approximation, $g_2(\tau)$ can be related to the field autocorrelation function, $g_1(\tau)$, using the Siegert relation:

$$g_2(\tau) = 1 + \sigma|g_1(\tau)|^2 \ , \tag{5}$$

where σ is the coherence factor, set by the specifics of the scattering setup (Borsali & Pecora, 2008). The motion of scatterers leads to a decorrelation and thus a decay in the correlation function. This decay is typically characterised by a distribution of relaxation times. For monomodal distributions the decay may be fitted with a stretched exponential function or a cumulant expansion (Schärtl, 2007), while multimodal distributions may be fitted using a sum of stretched exponential functions as:

$$g_1(\tau) = \sum_i A_i e^{-[\tau/\tau_i]^{\beta_i}} \ , \tag{6}$$

where A_i is the amplitude, τ_i the relaxation time, and β_i ($0 < \beta < 1$) the stretching parameter of the ith decay, respectively. The mean relaxation time $\langle\tau_i\rangle$ for a stretched exponential is:

$$\langle\tau_i\rangle = \frac{\tau_i}{\beta_i}\widetilde{\Gamma}\left(\frac{1}{\beta_i}\right) \ , \tag{7}$$

where $\widetilde{\Gamma}$ is the gamma function (Ioan, Aberle, & Burchard, 2001).

In dilute solutions, the dominant relaxation process on length-scales larger than the dispersed molecules or aggregates ($q \ll 1/R_g$) is due to translational diffusion. Here, the decay rate ($\Gamma_i \equiv 1/\langle\tau_i\rangle$) is $\Gamma = Dq^2$, where D is the diffusion coefficient. From D, the hydrodynamic radius R_h can be determined using the Stokes-Einstein relation:

$$D = \frac{k_B T}{6\pi\eta R_h} \ , \tag{8}$$

where k_B is the Boltzmann constant, T is the temperature, and η is the viscosity relevant for the diffusion.

At smaller length-scales ($q \gg 1/R_g$), internal molecular dynamics typically dominate, although translational diffusion can give contributions (Burchard & Richtering, 1989). Transitions from diffusive to internal motion behaviour can thus be observed as q is increased (Adam & Delsanti, 1977; Han & Akcasu, 1981; Sorlie & Pecora, 1988). In the internal motion regime, polymer subsections of size $L \sim 1/q$ are probed, which undergo diffusive dynamics with a diffusion coefficient that scales inversely with their size ($D \sim 1/L \sim q$), such that $\Gamma = Dq^2 \sim q^3$. This scaling can be derived more rigorously using the Zimm model, which leads to the relation (Adam & Delsanti, 1977; Berne & Pecora, 2000; Doi & Edwards, 1986; Dubois-Violette & de Gennes, 1967; Sorlie & Pecora, 1988; Witte et al., 2019):

$$\Gamma = \Lambda \frac{k_B T}{6\pi\eta_{app}} q^3 \ , \tag{9}$$

where Λ is a constant and η_{app} is the apparent viscosity (Adam & Delsanti, 1977; Doi & Edwards, 1986; Richter, Monkenbusch, Arbe, & Colmenero, 2005; Witte et al., 2019). Notably, the hydrodynamic radius of the scattering object can not be determined from DLS measurements in this regime, but one can determine the apparent viscosity experienced by the polymer subsections. The full Zimm prediction for the decay of $g_1(\tau)$ is an integral over exponential functions, which can be

approximated in different ways (Adam & Delsanti, 1977; Doi & Edwards, 1986; Richter et al., 2005), leading to somewhat different values of Λ. However, Λ is typically $\sim \mathcal{O}(1)$ and example values include 0.74 by Richter et al. (2005), 0.71 by Adam and Delsanti (1977), and 1.49 and 1.18 by Doi and Edwards (1986) (for good and θ solvent conditions, respectively).

Moreover, for fully dispersed neutral polymers in semidilute solutions, a relaxation arising from so-called cooperative diffusion is generally observed (Adam & Delsanti, 1977; Brown & Zhou, 1991; Burchard & Richtering, 1989; Cosgrove & Sutherland, 1983; Kanematsu, Sato, Imai, Ute, & Kitayama, 2005; Zettl et al., 2009). This relaxation is related to concentration fluctuations on the scale of the hydrodynamic correlation length, ξ_h, which in turn is approximately related to the static correlation length by the empirical relation $\xi_s \approx \xi_h/2$ (valid for semidilute solutions) (Brown & Nicolai, 1990; Uematsu et al., 2005; Uematsu, Svanberg, Nydén, & Jacobsson, 2003). The decay rate for cooperative diffusion is described by $\Gamma = D_{coop}q^2$, and the length-scale ξ_h may be calculated using the Stokes-Einstein relation: $D_{coop} = k_BT/6\pi\eta\xi_h$ (Uematsu et al., 2005). D_{coop} typically increases with increasing concentration (as ξ_h decreases, causing the characteristic decay time-scale to decrease) (Amis & Han, 1982; Burchard & Eisele, 1984; de Gennes, 1979; Uematsu et al., 2005; Yuan, Wang, Han, & Wu, 2006; Zettl et al., 2009). At high q, internal motions may still be probed in addition to the cooperative diffusion mode (Adam & Delsanti, 1977). We also note that additional modes have often been observed at slower time-scales, which have been attributed to various origins, such as clustering or aggregation, weak gelation, or the presence of dust or undissolved polymer (Li, Ngai, & Wu, 2010).

3. Materials and methods

3.1. Source material

A commercial LBG powder, typical of the quality used in industrial applications, (Seedgum C–175S, LBG Sicilia) was used. The powder was processed by the manufacturer using a chemical-free mechanical process to dehusk the seeds, separate the endosperm from the germ, and grind the endosperm into a powder. In appearance, the gum is a light yellow powder with visible brown specks.

3.2. Solution preparation

Milli-Q water was filtered twice using 200 nm pore size nylon membrane syringe filters. Stock solutions of 0.25 wt % LBG were prepared by dispersing LBG powder in the filtered Milli-Q water at room temperature under stirring, heating to 85 °C for 45 min under continued stirring, and leaving to cool to room temperature whilst stirring for a further 30 min. The stock solutions were then diluted to 0.05 wt % and left to stir overnight. At this stage, the solutions had a very slightly cloudy appearance with some visible impurities, which we expect were mainly non-polymeric material remaining from the powder manufacturing process. Thus, to enable a detailed characterisation, the LBG solutions were filtered to produce clear samples free of visible impurities.

We used a coarse filtration process to minimise influence on solution structure: the stock solutions were filtered using 5.0 μm and 1.2 μm syringe filters (surfactant-free cellulose acetate membrane) in sequence. The solution concentration following filtration was determined using density measurements with reference to a calibration curve, as described in Sec. 3.3. Following filtration, samples were prepared at a range of concentrations either by further dilution, or drying of the stock. Drying was achieved by rotary evaporation of filtered stock in a round-bottom flask (120 mPa, 57 °C, 70 rpm). The prepared solutions were clear at low concentrations, becoming very slightly turbid at the highest concentrations.

3.3. Density measurements

Density measurements were made on a batch of LBG solutions of known concentration (determined by drying and weighing of a high concentration sample). The resulting data were used to confirm the concentration of future batches through further density measurements.

These measurements were performed using a DMA 4500 M density meter (Anton Paar GmbH, Austria), on LBG solutions of concentration ranging from 0.01 to 0.21 wt %, at 25 °C. Measurements were performed in triplicate and the variation between repeat measurements was always less than 0.02 kg m^{-3}.

3.4. Polarimetry

The LBG galactose content was determined via polarimetry. Optical rotations were measured at the sodium D-line using a Schmidt + Haensch Polartronic H532 polarimeter, for LBG solutions with concentrations ranging from 0.1 to 0.37 wt % in a cell of 50 mm path length.

3.5. Shear rheology

Steady shear measurements were performed on LBG solutions with concentrations ranging from 0.006 to 0.86 wt %, using an MCR 302 stress-controlled rheometer (Anton Paar GmbH, Austria). A cone and plate geometry of 25 mm diameter and 1° pitch was used, equipped with a solvent trap to reduce evaporation. All measurements were made at 25 °C, and samples were left to equilibrate for 3 min before measurements were taken. Flow curves were measured using a stepped shear rate ramp. The range of accessible shear rates was limited by the minimum torque limit at low shear rates and secondary flow effects at high shear rates (Ewoldt, Johnston, & Caretta, 2015). The lowest LBG concentrations (0.01 wt %) were measured from 10–400 s^{-1}, while the highest concentrations (0.86 wt %) were measured from 0.01–1000 s^{-1}. The measurement duration at each step in the ramp was varied in proportion to the shear rate, from 60 s at the lowest shear rate to 15 s at the highest. Data were not recorded for the first 25% of each step, allowing for sample equilibration.

3.6. Static and dynamic light scattering (SLS and DLS)

Light scattering measurements were performed on LBG solutions at concentrations from 0.006 to 0.46 wt %, using a photon correlation spectrometer (LS Instruments AG, Switzerland) with a diode-pumped solid-state laser of vacuum wavelength $\lambda_0 = 660$ nm. Samples were placed in 10 mm diameter glass cuvettes and left in position to equilibrate for at least 30 min before measurements were performed. All measurements were made at 25 °C. A detector goniometer was used to perform measurements across the angular range of 24–110°, corresponding to scattering wavevectors of $q = 5.3$–20.7 μm^{-1}.

For SLS analysis, the excess Rayleigh ratio, $\Delta R(q)$, was determined from the sample scattering intensity, $I(q)$, using the reported Rayleigh ratio of toluene at $\lambda_0 = 660$ nm (Wu, 2010) as a reference. The sample refractive index, n, was estimated using the refractive index of water, a literature value of the refractive index increment ($dn/dc = 0.15$ mL g^{-1}, consistent with previously used and experimentally determined values) and the known solution concentration (Richardson, Willmer, & Foster, 1998; Richter, Boyko, Matzker, & Schröter, 2004; Sébastien et al., 2014).

Measurements were performed in pseudo-cross correlation mode, for which the signal from the detection optical fibre is split and received by two separate photon detectors; the two signals are cross-correlated to calculate the intensity autocorrelation function, $g_2(\tau)$, without interference from detector after-pulsing artifacts at short lag times. The absence of significant multiple scattering was confirmed by comparison with measurements made in the 3D correlation mode, which suppresses these effects. The pseudo-cross correlation mode was then chosen as it leads to

a greater signal to noise ratio and a wider dynamic range.

DLS data are presented, and were fitted, in the form $(g_2(\tau) - 1)/\sigma$, rather than following conversion to $g_1(\tau)$, as this conversion greatly amplifies noise at low correlation values.

3.7. Ultra-small-angle light scattering (USALS)

USALS measurements were performed on LBG solutions at concentrations from 0.01 to 0.86 wt %, using a HeNe laser light source with a vacuum wavelength of $\lambda_0 = 632.8$ nm, and a charge-coupled device (CCD) camera detector (Cipelletti & Weitz, 1999; Ferri, 1997). The intensity detected by the CCD was radially averaged to calculate intensity as a function of wavevector. This was then corrected for solvent scattering, cuvette scattering, and dark count intensity to find the excess scattering intensity of the sample, $I(q)$. Data were collected at a range of scattering wavevectors from roughly 0.07–1.2 μm^{-1}. Further data processing is detailed in Section VIA in the Supplementary Information (SI).

4. Results and discussion

LBG solutions were prepared following the procedure detailed in Section 3, with concentrations calculated based on the amount of water added in dilution, or lost during rotary evaporation, both of which were tracked by weight. Density measurements were performed on samples from 0.01 to 0.21 wt %, to confirm the accuracy of the concentrations determined by weight tracking. The measured densities are plotted against calculated LBG concentration in Fig. S1 (SI). The data are well described by a linear fit, confirming that the LBG concentration increased as expected upon drying and that the weight measurements yielded accurate results. The density of solutions at higher LBG concentrations were not measured due to the high solution viscosity, which hinders the proper cleaning of the density meter capillary.

Optical rotation as a function of LBG concentration is shown in Fig. S2 (SI). A linear fit was performed with the intercept fixed at the origin, and the calculated gradient used, along with the path length, to calculate the specific rotation, $[\theta_\alpha]_D = 14.8 \pm 0.5$. A calibration from literature was then used to determine the corresponding M:G value (Noble, Perez, Rochas, & Taravel, 1986). Our own re-analysis of the literature dataset found the calibration curve as $[\theta_\alpha]_D = (267 \pm 13)\varphi_G - (45 \pm 4)$, where φ_G is the galactose molar fraction. The resulting value of M:G was (3.4 ± 0.3):1.

In the following subsections we present the results of the steady state shear rheology, SLS, USALS, and DLS.

4.1. Viscosity scaling

Representative flow curves, i.e. viscosity η versus shear rate $\dot{\gamma}$, spanning the investigated range of LBG concentrations are shown in Fig. 2. For the lowest concentrations ($\lesssim$ 0.05 wt %), the viscosity is relatively constant within the range of measured shear rates, while shear thinning behaviour is clearly observed at higher concentrations. Where shear thinning behaviour is observed, the viscosity is seen to approach a plateau at low shear rates and fall off at high shear rates, following approximately power law behaviour. The viscosity at all shear rates, and the slope within the shear thinning region, are both observed to increase with concentration.

To further investigate the concentration dependence, each flow curve was fitted using a modified form of the Carreau-Yasuda model (Vlassopoulos & Schowalter, 1994):

$$\eta(\dot{\gamma}) = \eta_0(1 + (\tau_\lambda \dot{\gamma})^a)^{(n-1)/a}, \quad (10)$$

with three free parameters: the zero-shear viscosity, η_0, the relaxation time, τ_λ, and the power law index, n. The transition width, a, was fixed to 0.75; this was found to satisfactorily fit each curve and allowed for more stable fitting of the remaining free parameters. A brief discussion of the fitted values of τ_λ and n is given in the SI—in the following sections we focus on the zero-shear viscosity data.

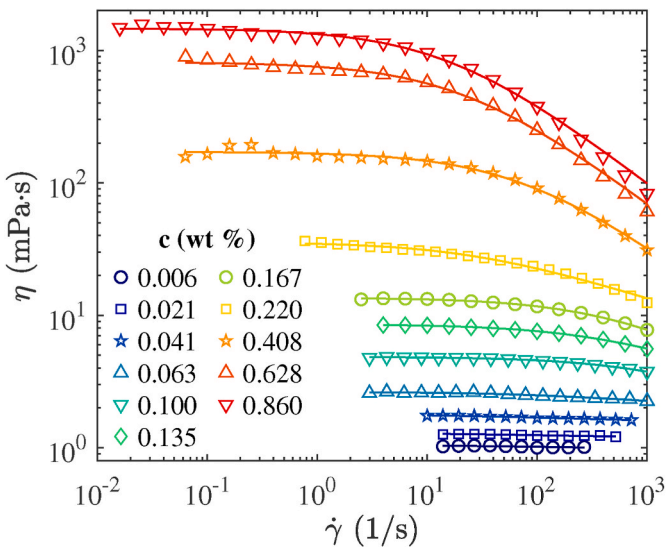

Fig. 2. Representative flow curves (viscosity, η, against shear rate, $\dot{\gamma}$) spanning the range of LBG concentrations measured. Solid lines are fits to the modified Carreau-Yasuda model.

The intrinsic viscosity $[\eta]$ was determined by performing a Huggins-Kramer double extrapolation (Fig. S5 (SI)). The Huggins and Kramer equations are linearisations, valid at low concentrations, of the inherent viscosity, $\eta_{inh} = \ln(1 + \eta_{sp})/c$ (where η_{sp} is the specific viscosity), and reduced viscosity, $\eta_{red} = \eta_{sp}/c$, respectively. The two linearisations share the intrinsic viscosity as a common intercept ($\eta_{inh}(c = 0) = \eta_{red}(c = 0) = [\eta]$), so η_{inh} and η_{red} were fitted simultaneously using a unified intercept, resulting in the intrinsic viscosity $[\eta] = 1660 \pm 30$ mL g^{-1} (16.6 ± 0.3 $(wt\%)^{-1}$), consistent with values previously reported for LBG (Dakia et al., 2008; Goycoolea, Morris, & Gidley, 1995; Launay et al., 1997; Picout, Ross-Murphy, Jumel, & Harding, 2002; Richardson et al., 1998).

The Mark-Houwink equation, $[\eta] = KM^\alpha$, allows for an estimate of the molecular weight of a polymer based on its intrinsic viscosity in solution, given the constants K and α for the particular polymer-solvent system (Rubinstein & Colby, 2003). The parameter α characterises the structure of the polymer in solution and is directly related to the fractal dimension, d_f, and scaling exponent, ν, by $\alpha = 3\nu - 1 = (3/d_f) - 1$ (Rubinstein & Colby, 2003). The Zimm model predicts $\alpha = 0.5$ ($d_f = 2$, $\nu = 0.5$) for polymers in θ solvent conditions, and $\alpha = 0.76$ ($d_f = 1.7$, $\nu = 0.588$) for good solvent conditions (Rubinstein & Colby, 2003). A review of reported $[\eta]-M$ datasets for various galactomannans in water found that the exponent α was consistent, within experimental uncertainty, so long as a proper solubilisation method had been followed (Picout & Ross-Murphy, 2007); the exponents found were all in the range $0.70 < \alpha < 0.75$, suggesting that galactomannans are generally in good, or close to good, solvent conditions in water. An earlier study (Picout et al., 2002) included a unified fit over a number of such datasets, finding $\alpha = 0.74 \pm 0.01$, and our re-analysis of these data yielded $K = 0.040 \pm 0.001$ mL g^{-1} (Picout et al., 2002). Using these Mark-Houwink parameters, characteristic of LBG solutions in water, together with our measured intrinsic viscosity, we determine the (weight-averaged) molecular weight of our LBG sample as $M_w = 1700 \pm 500$ kDa. The coil size may be estimated using the Flory-Fox equation: $\langle R_{ee}^2 \rangle^{3/2} = M[\eta]/\Phi$, where R_{ee} is the end-to-end distance, and $\Phi = 2.5 \times 10^{23}$ mol^{-1} is a constant (Rubinstein & Colby, 2003). In turn, this may be used to estimate the radius of gyration (R_g), since for a linear polymer in θ solvent conditions, $\langle R_g^2 \rangle = \langle R_{ee}^2 \rangle/6$ (Rubinstein & Colby, 2003). We find $R_{ee} = 224 \pm 22$ nm and $R_g = 92 \pm 9$ nm, close to previously determined values for LBG (Picout et al., 2002).

The specific viscosity, $\eta_{sp} = (\eta_0 - \eta_s)/\eta_s$, where η_s is the solvent viscosity, was determined and is shown versus reduced concentration, $c[\eta]$, in Fig. 3. We identify three distinct scaling regimes, and assign these as the dilute, semidilute unentangled, and semidilute entangled regimes, respectively, although we note that the semidilute unentangled spans a narrow range of concentration. The data within each regime were well described using power laws of the form $\eta_{sp} \sim c^{\zeta}$, and were fitted with regression lines for determination of the scaling exponents and crossover concentrations. We find $\zeta = 1.03 \pm 0.07$, 1.65 ± 0.05, and 3.0 ± 0.1, within the dilute, semidilute unentangled, and semidilute entangled regimes, respectively. The transition from dilute to semidilute solutions occurs at the overlap concentration, $c^*[\eta] = 0.52 \pm 0.08$ ($c^* = 0.031 \pm 0.005$ wt %), with $\eta_{sp}(c^*[\eta]) = 0.64 \pm 0.12$, and that from unentangled to entangled solutions occurs at the entanglement concentration, $c^e[\eta] = 2.1 \pm 0.2$ ($c^e = 0.13 \pm 0.02$ wt %), with $\eta_{sp}(c^e[\eta]) = 6 \pm 2$. The viscosity values at the overlap and entanglement concentrations are consistent with typically observed values (roughly twice the solvent viscosity at overlap, >10 times the solvent viscosity at c^e) (Colby, 2010), supporting the identification of these regimes.

For neutral polymers in good solvents, the semidilute unentangled regime typically spans roughly one decade in concentration ($c^e/c^* \approx 10$), while in θ conditions, the regime is expected to be increasingly compressed as molecular weight is increased (Colby, 2010). Indeed, for polymers in poorer solvent conditions, the regime is often very narrow or not clearly observed at all (Colby, 2010; Dumitriu, 2004). The observed regime width, $c^e/c^* \approx 4$, therefore appears consistent with a neutral linear polymer in solvent conditions somewhere between those of θ and good solvents. Such a compression of the semidilute unentangled regime is commonly observed for aqueous polysaccharide solutions (Dumitriu, 2004).

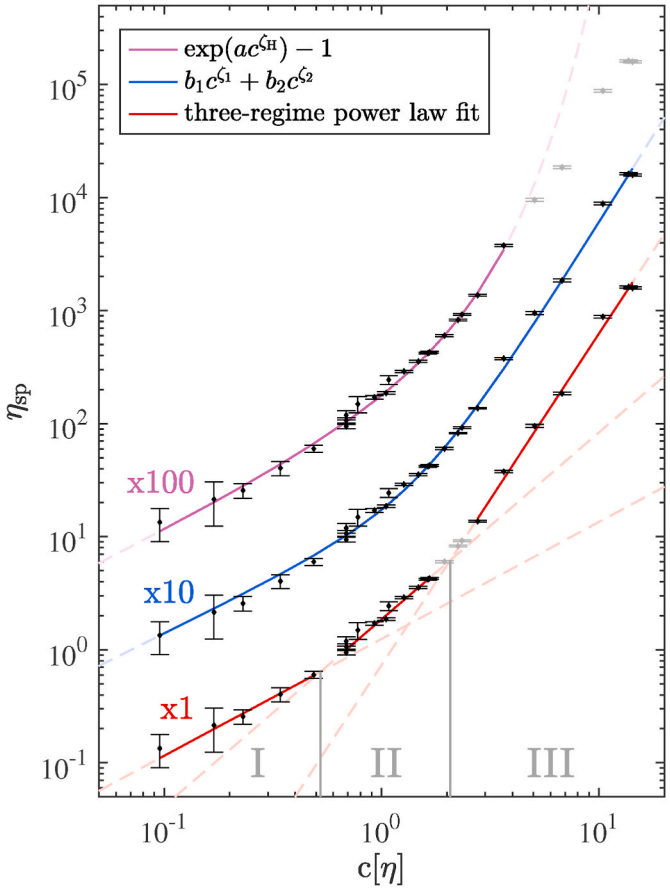

Fig. 3. Specific viscosity, η_{sp}, against reduced concentration, $c[\eta]$. Error bars indicate 95% confidence intervals. Solid red lines are piecewise power law fits, each fitted to the data they span, with dashed red lines showing extrapolations of these power laws. Grey vertical lines mark the two crossover points, determined as the intersections between neighbouring power law fits, thus marking the boundaries of the three identified regimes: I (dilute), II (semidilute unentangled), and III (semidilute entangled). The solid blue line denotes a fit using the sum of two power laws, and the solid purple line denotes a fit to the stretched exponential form arising from a hydrodynamic scaling approach (see discussion in the text) and the dashed purple line shows the extrapolation of this fit. The data for the latter two fitting approaches are shifted vertically by factors of 10 and 100, respectively, for clarity. For each fitting approach, excluded data are denoted by light grey data points.

Considering the narrow span of the middle regime, we also considered a fitting approach based on the sum of two power laws ($\eta_{sp} = b_1c^{\zeta_1} + b_2c^{\zeta_2}$, where b_i are the amplitudes and ζ_i the scaling exponents of the two regimes, respectively, as shown in Fig. 3). Here, the whole dataset is fitted with a continuous expression, and the intermediate concentrations are considered a transition between the dilute and entangled regimes. This approach proved fairly successful, with the exponents $\zeta_1 = 1.0 \pm 0.2$ and $\zeta_2 = 3.1 \pm 0.1$ (consistent with those found for the dilute and semidilute entangled regimes of the three-regime-framework). We also fitted the data using the stretched exponential form predicted by the hydrodynamic scaling theory (Eq. (1)). As shown in Fig. 3, this form describes the LBG data well, with $a = 1.02 \pm 0.02$ and $\zeta_H = 0.97 \pm 0.02$, from the lowest concentrations measured up to $c[\eta] \sim 4$ ($\eta_{sp} \sim 55$), beyond which the data require a power law description. The transition from stretched exponential to power law behaviour typically occurs at higher (and sometimes significantly higher) values of both concentration and viscosity, although we note a study on 1000 kDa hydroxypropylcellulose which was described using the same approach, finding highly similar values ($a = 0.97$ and $\zeta_H = 0.93$, with a stretched exponential to power law transition at $c[\eta] \sim 4$, with $\eta_{sp} \sim 90$) (Phillies, 2011; Phillies & Quinlan, 1995). In summary, the viscosity scaling data may be satisfactorily described by a number of approaches: as a stretched exponential growth (up to $c[\eta] \sim 4$, beyond which a power law is required), as a sum of two power laws with a continuous transition between these, or as three distinct power law regimes. In the following sections, we focus on the parameters found for the three-regime approach in order to compare our results both to theoretical expectations, and to literature values determined using this framework.

The scaling exponent in the dilute regime ($\zeta = 1.03 \pm 0.07$) is consistent with $\zeta = 1$, as predicted by the Zimm model for linear flexible neutral polymers. The value in the semidilute unentangled regime ($\zeta = 1.65 \pm 0.05$) is between the Rouse model predictions of $\zeta = 1.3$ for good conditions and $\zeta = 2.0$ for θ solvent conditions. For solvent conditions between these two bounds, the exponent in the Rouse model is given by $\zeta = 1/(3\nu - 1)$ (Colby, 2010); our measured value thus corresponds to $\nu = 0.54 \pm 0.01$. The Mark-Houwink parameter discussed above, $\alpha = 0.74$, corresponds to $\nu = 0.58$, so the two results are comparable. The slope in the entangled regime ($\zeta = 3.0 \pm 0.1$) is lower than the theoretically expected values, which are $\zeta = 4.7$ for θ conditions and $\zeta = 3.9$ for good solvent conditions (Colby, 2010).

An influential early study by Morris et al. (1981) interpreted viscosity scaling data for LBG, guar gum, and a range of other polysaccharides in terms of only two regimes—dilute and semidilute, although the term 'concentrated' was used instead of semidilute. Many subsequent studies of galactomannans have used this framework (Andrade et al., 1999; Doyle et al., 2009; Gillet et al., 2017; Hellebois et al., 2021; Pollard & Fischer, 2014; Wientjes, Duits, Jongschaap, & Mellema, 2000). We found only one previous study on LBG which recognised a need to split the semidilute regime into unentangled and entangled regimes (Launay et al., 1997). This complicates literature comparisons and interpretations, as the three-regime-framework has two transition concentrations (c^* and c^e), while the two-regime-framework only involves one, also generally termed c^*, with a value that lies between the two identified from a

three-regime-analysis. Using the two-regime-framework, the fitting range for the lower regime may cover dilute concentrations as well as much of the semidilute unentangled range, leading to an enhanced scaling exponent. Furthermore, our own re-analysis of Morris et al. (1981) suggests that most of the data fitted as part of the 'dilute' regime actually occupied the semidilute unentangled regime (for LBG, the range was $c[\eta] = 0.5–3.1$), such that the exponent obtained would be more appropriately compared to predictions and literature for the semidilute unentangled regime. Similar enhancement of the dilute regime scaling can be seen in more recent studies using the two-regime-framework; for example, see Doyle et al. (2009) and Hellebois et al. (2021). The more the fitted concentration range represents the dilute range, the lower this effect will be; it may be avoided altogether in two-regime analyses by considering the intermediate concentrations as a broad transition region and excluding them. For the high concentration regime in the two-regime-framework, the fitting range typically matches the semidilute entangled regime quite well; this makes comparisons between studies more straightforward, regardless of the framework used.

In the dilute regime, scaling exponents of ~ 1.1–1.2 have been found for LBG (Andrade et al., 1999; Launay et al., 1997; Richardson et al., 1998). In the semidilute entangled regime, Morris et al. (1981) found $\zeta \approx 3.9$ for LBG (and guar gum), while they found $\zeta = 3.3 \pm 0.3$ for other investigated polysaccharides. This enhanced scaling was attributed to the presence of intermolecular interactions which the authors termed 'hyperentanglements', although we note that the reported value is consistent with the expected value for entangled solutions of flexible neutral polymers. Other studies on LBG have found exponents of $\zeta \approx$ 3.7–4.8 (Andrade et al., 1999; Doublier & Launary, 1981; Gillet et al., 2017; Launay et al., 1997; Sittikijyothin et al., 2005), again generally consistent with theoretical predictions for entangled solutions. In the semidilute unentangled regime, Morris et al. (1981) found a scaling exponent of 1.4, while in the study by Launay et al. (1997) a three-regime-analysis on LBG solutions found exponents of $\zeta = 1.16$, 1.9, and 4.0, respectively, with transition concentrations of $c^*[\eta] = 0.76$ and $c^e[\eta] = 3.56$. These results are quite consistent with ours, apart from the slope in the entangled regime, which is noticeably higher than our determination and closer to the theoretically expected value. However, we note that neither our results, nor those of other studies (Andrade et al., 1999; Doublier & Launary, 1981; Gillet et al., 2017; Launay et al., 1997; Morris et al., 1981; Sittikijyothin et al., 2005), show evidence for so-called 'hyperentanglements' based on the scaling exponent within the entangled regime. The same holds for many studies on other galactomannans (Andrade et al., 1999; Pollard & Fischer, 2014; Sittikijyothin et al., 2005), including those nearly fully substituted with galactose (M:G ~ 1:1) (Doyle et al., 2009; Ganter et al., 1992; Hellebois et al., 2021).

4.2. Static light scattering (SLS)

SLS measurements were performed for LBG concentrations ranging from 0.006 to 0.83 wt %, thus spanning the concentration regimes observed in the viscosity data. Representative profiles of the excess Rayleigh ratio $\Delta R(q)$ as a function of scattering wavevector are shown in Fig. 4.

For all concentrations, $\Delta R(q)$ decreases with q, and exhibits approximately a power law scattering profile, which suggests that the scattering is mainly due to the internal structure of self-similar scattering objects. The results also demonstrate that these structural characteristics persist across the entire probed range of q, corresponding to length-scales ≈ 50–170 nm ($1/q_{max}$–$1/q_{min}$). The lack of any roll-off to a plateau at low q indicates that the objects themselves are characterised by a length-scale greater than roughly 170 nm. This is much larger than the expected R_g for a single LBG coil (as discussed above, our estimate from the Flory-Fox relationship, assuming an ideal chain, was $R_g = 92 \pm$ 9 nm), suggesting that scattering from supramolecular aggregates dominates over that from fully dispersed LBG. Indeed, early attempts to

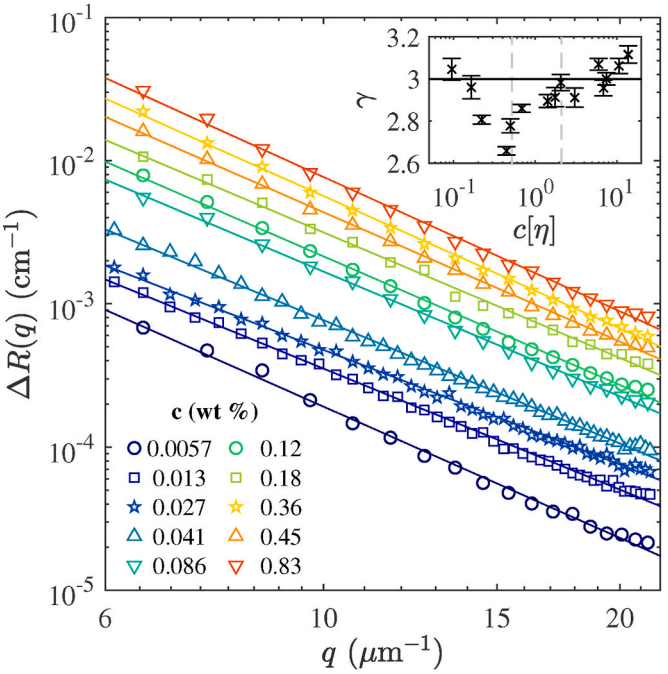

Fig. 4. Excess Rayleigh ratio, ΔR, against scattering wavevector, q, from SLS measurements. Solid lines are linear fits. The inset shows the negative of the fitted slopes, γ, against reduced concentration, $c[\eta]$ (error bars indicate 95% confidence intervals). Grey dashed lines denote the regimes identified from steady shear rheology: I (dilute), II (semidilute unentangled), and III (semidilute entangled). The solid black line indicates $\gamma = 3$.

determine the molecular weight of LBG using light scattering (via the Zimm plot method) were rendered unsuccessful due to similar aggregation effects (Doublier & Launary, 1981; Gaisford et al., 1986).

In contrast to this behaviour, the $\eta_{sp}(c)$ results, discussed above, are generally consistent with expected behaviour for well-dispersed flexible polymers (except for the somewhat lower ζ value observed in the semidilute entangled regime), demonstrating that the molecular aggregates observed in SLS are, at most, weakly affecting the viscosity results, which instead mainly probe the well-dispersed polymer fraction.

The SLS data were fitted with power laws of the form $\Delta R(q) = Aq^{-\gamma}$, and the fitted γ values are shown in the inset to Fig. 4. We find that γ is relatively similar across the measured concentration range, with values within the range 2.66–3.12 and a mean value (across all concentrations) of $\langle\gamma\rangle_c = 2.9 \pm 0.1$. We note that a small dip in the data is observed within the dilute concentration range around 0.02 wt %, as shown in the inset. We are not sure of its origin, but note that in addition to the scattering from aggregates, we expect to also have a contribution from the dispersed polymer fraction and as c increases this could lead to a variation in the determined γ, where one could imagine c-dependent changes both to the number density and compactness of the aggregates and to the scattering contribution from the dispersed fraction.

It is not clear whether the relatively high value of $\gamma = 2.9$ should be interpreted as the fractal dimension d_f of the aggregates. High power law exponents ~ 3–4 can arise from surface scattering, and are observed e.g. in gels and network-forming systems with dense, porous structures (Bhatia, 2005; Ioannidou et al., 2016). Thus, power law-like scattering could be observed not only for fractal structures, but as a result of the averaging over complex structures, particularly when a limited range of length-scales is probed.

To further investigate the concentration dependence of the scattering, the excess Rayleigh ratio at fixed scattering angles are plotted versus c in Fig. S6 (SI). Across all scattering angles, the scattered intensity increases with c, roughly following a power law $\Delta R(q) \sim c^e$. The data for each scattering angle were fitted with a power law fit to

determine the exponent ε, which is plotted as a function of scattering angle in the inset. ε is consistent across the angular range, with a mean value of $\langle\varepsilon\rangle_\theta = 0.77 \pm 0.01$. Thus, we do not find evidence from the SLS data of any c-dependent structural transitions in the growth of the excess Rayleigh ratio with c for fixed scattering angles, which is consistent with the lack of any significant c-dependence in the power law exponents γ. This lack of c-dependence stands in direct contrast to the viscosity behaviour which demonstrates three distinct concentration regimes. We interpret these observations as due to the fact that the scattering is dominated by aggregates which remain relatively unchanged in characteristics with varying c. The relatively high value of γ, and the fact that a consistent behaviour is found also for the lowest investigated concentrations within the dilute regime, and for length-scales of at least 170 nm, demonstrates the presence of relatively compact aggregates of size > 170 nm.

4.3. Ultra-small-angle light scattering (USALS)

USALS measurements were performed for LBG concentrations ranging from 0.01 to 0.86 wt %. The recorded scattering intensity in excess of the solvent scattering is shown as a function of scattering wavevector q in Fig. 5. Data are shown renormalised by concentration, although an additional arbitrary intensity rescaling was required for the 0.07 and 0.86 wt % data, in order for the data to overlay the other concentrations.

The excess scattering profiles are qualitatively similar across all measured concentrations, displaying approximately power law scattering at low q ($\lesssim 0.2\ \mu m^{-1}$), followed by a flattening into a plateau-like region at higher q (approximately 0.2–1 μm^{-1}), and then decreasing more steeply once again at the highest probed q values ($\gtrsim 1\ \mu m^{-1}$). Overall, the scattering decreases with q across the entire probed range (corresponding to length-scales $\approx$ 0.75–14 μm). As for SLS, the lack of a roll-off at low q indicates the presence of structures larger than the largest probed length-scales, i.e. larger than $\sim$ 14 μm. This provides evidence for the presence of very large supramolecular structures, at least 100 times greater than the R_g of a single LBG coil (estimated to be $\approx$ 100 nm (Picout et al., 2002)).

The largest q probed by the USALS measurements was $\sim 1.3\ \mu m^{-1}$, and the smallest q probed with SLS was $\sim 6\ \mu m^{-1}$, leaving an unexplored gap of roughly two thirds of an order of magnitude for which the scattering profile is not known, although we note that the steeper decrease observed in the high-q USALS region appears consistent with a transition to the power law profiles observed in SLS. It is thus reasonable to expect a smooth transition between the two measurements, with the intensity fall-off at $\gtrsim 1\ \mu m^{-1}$ indicating the start of this transition. The flattening in the mid-q region demonstrates the clear separation of the two power law regimes, suggesting two separate populations of aggregated structures.

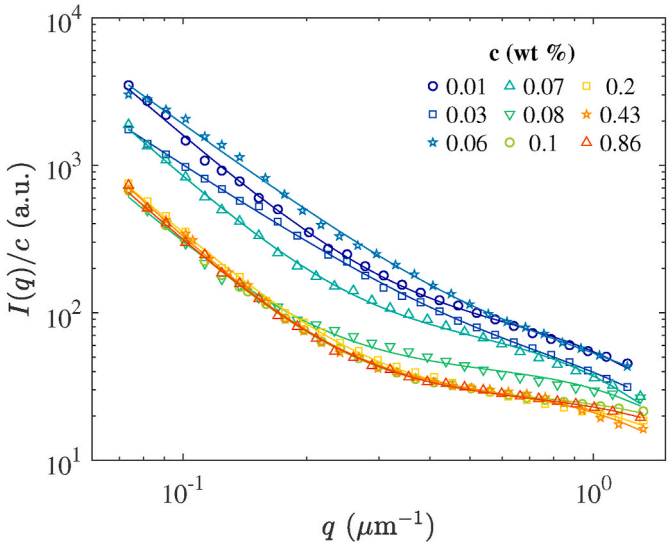

Fig. 5. Renormalised excess scattering intensity, $I(q)/c$, versus scattering wavevector, q, from USALS measurements. Solid lines are fits to a sum of a power law and a modified Lorentzian. An additional intensity rescaling has been applied to the 0.07 and 0.86 wt % data.

To investigate the results further, the data were fitted to a sum of a power law and a modified Lorentzian function (Hammouda, Ho, & Kline, 2004; Witte et al., 2019), where the latter was chosen as a simple empirical function that can describe the data:

$$I(q)/c = A_1/q^{\gamma_1} + A_2/(1+(lq)^{\gamma_2}) \ , \tag{11}$$

where A_1 is the amplitude and γ_1 the exponent of the low-q power law; A_2 is the amplitude and γ_2 the exponent of the high-q power law; and l is the length-scale of the modified Lorentzian. The high-q power law slope is not clearly observed, as the transition is close to the end of the measurement window; thus, the high-q exponent γ_2 was set to 2.9, chosen to match the average power law exponent observed by SLS ($\langle\gamma\rangle_c = 2.9 \pm 0.1$), whereas A_1, γ_1, A_2, and l were allowed to vary as free parameters.

The data were well fitted by this expression and the resulting fitting parameters are shown in Fig. S7 (SI). γ_1 was generally found to be $\sim$ 2.4–2.6, although the 0.03 and 0.06 wt % solutions showed smaller exponents of $\sim$ 1.8 and 2.0, respectively. The mean value across all concentrations was $\langle\gamma_1\rangle_c = 2.4 \pm 0.3$. Thus, the low-$q$ exponent is somewhat smaller than that observed for the power law in the high-q SLS region. The estimated transition length-scale may offer further insight: we obtained $l \sim$ 500–900 nm, with an average over all investigated concentrations of $\langle l\rangle_c = 670 \pm 140$ nm. Notably, this length-scale is consistent with the filtration pore size ($\sim$ 600 nm radius) used in our sample preparation. Thus, we hypothesize that prior to filtration, LBG forms aggregates of a size generally larger than the filter pores, but the filtration yields aggregates of $\sim$ 600 nm radius. We also hypothesize that these filtration-defined 'primary' aggregates can undergo further aggregation and form larger structures, as observed in the experiments. If we interpret both power law-regimes as due to scattering from fractal structures, the data indicate a more open and less dense aggregated structure on larger length-scales.

To further investigate the primary aggregates, we note that the observation of a roll-off of the scattering, resulting from these aggregates, onto an intermediate plateau, suggests the use of a Zimm plot analysis (Borsali & Pecora, 2008; Rubinstein & Colby, 2003) to determine the corresponding aggregate molecular weight. Thus, a Zimm plot was constructed using scattering data from the upper end of the USALS q-range for the 0.01 and 0.03 wt % LBG samples, as shown in Fig. S8. The resulting molecular weight was $M_w = 1.5 \times 10^{10}$ g mol^{-1} (1.5×10^7 kDa), which is $\sim 10^4$ times larger than the polymer molecular weight determined by the intrinsic viscosity determination, and may be interpreted as the molecular weight of these primary aggregates.

In a previously published SLS and USALS study, aqueous solutions of guar gum (another galactomannan) were prepared without filtration (instead using a purification procedure that consisted of dissolution, centrifugation, precipitation, drying, and grinding), finding evidence of large structures with characteristic lengths of tens of microns (Gittings et al., 2000). SLS demonstrated power law-like scattering which continued in the USALS regime, without an intermediate plateau, until a roll-off into a low-q plateau took place (the measurements extended down to 0.015 μm^{-1}). The formation of such large structures for guar gum lends further support to the suggestion that LBG forms similarly large structures upon dissolution, which due to filtration, however, give rise to the more complex structure observed here, with an intermediary plateau.

Finally, we note an apparent concentration-grouping in the renormalised data (Fig. 5); the data appear to collapse into two groups, with

lower concentrations (below ~ 0.07–0.08 wt %, $c[\eta]$ ~ 1.2–1.3) showing a higher renormalised intensity than higher concentrations. The separation is increasingly apparent at lower q-values. This suggests that the degree of aggregation displayed on the larger length-scales is higher in the lower concentration solutions.

4.4. Dynamic light scattering (DLS)

Intensity autocorrelation functions $g_2(\tau)$ were measured for LBG concentrations ranging from 0.01 to 0.46 wt %. Fig. 6 shows $(g_2(\tau)-1)/\sigma$ versus lag-time τ, for scattering angles of (a) $\theta = 30°$ ($q = 6.6\ \mu m^{-1}$), and (b) $\theta = 100°$ ($q = 19.4\ \mu m^{-1}$). For most of the probed concentrations ($c \leq 0.14$ wt %, $c[\eta] \leq 2.1$), the data show a single decay mode, here termed 'slow', while at high concentrations ($c \geq 0.22$ wt %, $c[\eta] \geq 3.2$) a secondary mode that occurs at shorter time-scales than the primary decay, here termed 'fast', is also observed; the fast mode is more apparent at higher scattering angles, corresponding to higher q and thus shorter length-scales. It is clearly observed that the slow relaxation occurs at increasingly long time-scales as c is increased.

For a quantitative study of the variation of the observed relaxations with concentration, the data were fitted using either a single stretched exponential, or a sum of two stretched exponential functions. For concentrations of 0.14 wt % or below, where only a single relaxation decay was observed, a single stretched exponential function was used:

$$(g_2(\tau)-1)\Big/\sigma = (\exp(-[\tau/\tau_s]^{\beta_s}))^2\ , \tag{12}$$

with two free parameters: the decay time-scale, τ_s, and the stretching parameter, β_s. The stretching parameter may take values between 0 and 1, where a value of 1 corresponds to a simple, non-stretched, exponential. For concentrations of 0.22 wt % and above, where a faster secondary mode was also observed, data were fitted with a sum of two stretched exponential functions:

$$(g_2(\tau)-1)\Big/\sigma = (A_f\exp(-[\tau/\tau_f]^{\beta_f}) + (1-A_f)\exp(-[\tau/\tau_s]^{\beta_s}))^2\ , \tag{13}$$

with five free parameters: the time-scales, τ_f and τ_s, and stretching parameters, β_f and β_s, of the fast and slow relaxations, respectively, and the fast mode amplitude, A_f (the slow mode amplitude was constrained as $A_s = 1 - A_f$). Mean relaxation times were calculated for each mode using Eq. (7). This fitting approach generally described the data well, as shown by the solid lines in Fig. 6.

The amplitudes resulting from the combined fitting of the fast and slow relaxation modes are shown as a function of q in Fig. S9 (SI), for the three concentrations where the fast mode was observed. The amplitude of the slow mode increases with concentration and decreases with q, whereas A_f decreases with concentration and increases with q (being very low for the lowest probed q). This reflects the different length-scales characterising the two contributions: we expect the slow mode to be associated with scattering from larger objects as compared to the fast mode.

We next use these amplitudes, determined by DLS, to determine the contributions to the SLS scattering profiles from the structures associated with the fast and slow relaxation modes, respectively. The contribution to the total excess Rayleigh ratio from the fast mode, ΔR_f, is given by:

$$\Delta R_f = \frac{A_f \Delta R}{A_f + A_s}, \tag{14}$$

where $A_f + A_s = 1$. The contribution from the slow mode, ΔR_s, is determined similarly, and $\Delta R_f + \Delta R_s = \Delta R$. The two contributions are plotted, renormalised by concentration, in Fig. S10 (SI). It is clear that the dominant scattering contribution comes from aggregate structures associated with the slow mode, and that the fast mode does not contribute strongly to the SLS results, particularly at low q. We also note that ΔR_f is relatively insensitive to q compared with the slow mode contribution.

4.4.1. Fast mode

Due to the low amplitude of the fast modes, the stretching parameters resulting from free fits were generally noisy and showed no clear trend with regards to a variation of q. Thus, the fits were instead performed using fixed q-independent values of β_f, based on the average of the values of $\beta_f(q)$ obtained from the free fitting procedure. The values chosen were: $\beta_f = 0.85$ for $c = 0.22$ wt % and $c = 0.3$ wt %, and $\beta_f = 0.70$ for $c = 0.46$ wt %.

The mean decay time-scales $\langle\tau_f\rangle(q)$ are shown in Fig. S11 (SI). We find that $\langle\tau_f\rangle(q)$ is relatively c-independent, and note that the fast mode appears within the entangled semidilute c-regime. However, given the weakness of the fast mode contribution it is difficult to pinpoint with any accuracy the c-regime where the fast mode originates. The fast mode decay rates ($\Gamma_f = \langle\tau_f\rangle^{-1}$) could be well described as proportional to q^2 (Fig. S12 (SI)), demonstrating diffusive behaviour. Diffusion coefficients (D_f) were determined for each concentration as the slope of linear fits to these data ($\Gamma_f = D_f q^2$), with an average value of $\langle D_f\rangle_c = 5.8 \pm 0.3$

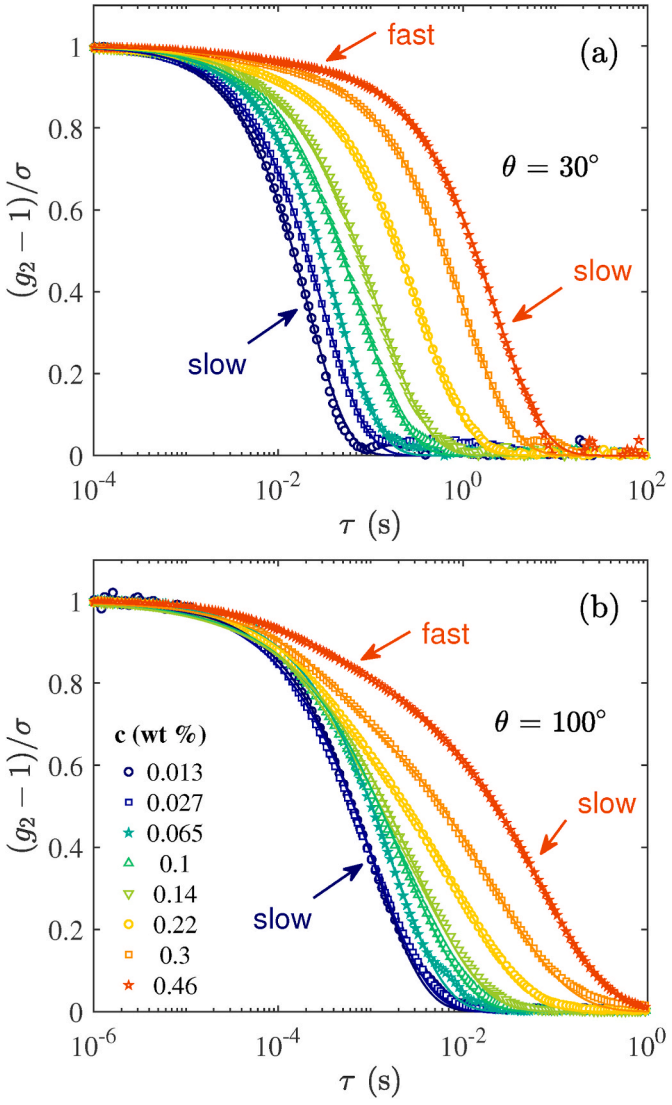

Fig. 6. Intensity autocorrelation functions ($(g_2-1)/\sigma$ against lag time, τ) from DLS measurements performed at scattering angles of (a) 30° and (b) 100°. Solid lines are fits to single stretched exponential functions for $c \leq 0.14$ wt %, and double stretched exponential functions for $c \geq 0.22$ wt %.

$\mu m^2\ s^{-1}$.

The diffusion coefficient for each concentration was also used to determine an apparent hydrodynamic radius corresponding to the fast mode, $R_{h,f}$, using the Stokes-Einstein relation. We expect that the viscosity experienced by this relaxation mode will be situated somewhere between that of the pure solvent and the bulk solution; thus, these two values were used to provide limiting values to $R_{h,f}$. Using $\eta = \eta_s$, and averaging over c, provides an upper limit of $\langle R_{h,f}\rangle_c = 42 \pm 2$ nm. Using $\eta = \eta_0$ provides lower limits of $R_{h,f}$, varying from ~ 2.7 to ~ 0.3 nm as $c[\eta]$ varies from 3.2 to 6.8.

The fact that the fast mode is (i) associated with the dispersed LBG phase, (ii) diffusive, (iii) characterised by a relatively fast decay time-scale, corresponding to a relatively small length-scale, and (iv) observed within the semidilute regime, strongly suggests that it is due to cooperative diffusion. Cooperative diffusion is typically expected to arise within the semidilute unentangled regime (Burchard & Richtering, 1989; de Gennes, 1979); however, as discussed above, the weakness of the fast mode contribution makes it difficult to pinpoint where it originates. Furthermore, the similarity of D_f across the measured concentrations is somewhat unexpected, as the cooperative diffusion coefficient is generally expected to increase with increasing c, as the correlation length decreases (Amis & Han, 1982; Burchard & Eisele, 1984; de Gennes, 1979; Uematsu et al., 2005; Yuan et al., 2006; Zettl et al., 2009); however, the measured concentrations might not be high enough to observe this.

We note a study of hydrophobically-modified polyoxyethylene in water (Nyström, Walderhaug, & Hansen, 1993), for which a fast mode attributed to cooperative diffusion exhibited a decreasing time-scale above the crossover concentration, to a plateau value of roughly 2 ms at $q \approx 9\ \mu m^{-1}$ for $c \gtrsim 2c^*$. At a similar scattering wavevector ($\theta \approx 40°$), the values of $\langle\tau_f\rangle(q)$ observed here are ~ 1.5–3 ms (Fig. S11 (SI)). Thus, our observations show similarity to this study both in the magnitude of the fast decay time-scale as well as the approximate independence of this mode on concentration in semidilute solutions.

Values of D_{coop} for typical systems include ~ 0.02–20 $\mu m^2\ s^{-1}$ for polystyrene in dioctyl phthalate (Nicolai & Brown, 1996), or ~ 16–160 $\mu m^2\ s^{-1}$ for polystyrene in tetrahydrofuran (Amis & Han, 1982). The value found here ($\langle D_f\rangle_c = 5.8 \pm 0.3\ \mu m^2\ s^{-1}$) falls well within this typical range. Using the cooperative diffusion interpretation, the characteristic size determined using the Stokes-Einstein relation (with solvent viscosity as an approximation of the local viscosity) represents the hydrodynamic correlation length, ξ_h. Using the empirical relation $\xi_s \approx \xi_h/2$ (Brown & Nicolai, 1990; Uematsu et al., 2003), we calculate the static correlation length as $\xi_s \approx 21$ nm, in fairly good agreement with results from a previous Small Angle X-ray Scattering (SAXS) experiment on a solution of 0.2% LBG in water, which found $\xi_s = 27$ nm (Turquois, Rochas, Taravel, Doublier, & Axelos, 1995).

In conclusion, our observations support that the fast relaxation mode is due to cooperative diffusion and thus concentration fluctuations on the length-scale of the hydrodynamic correlation length.

4.4.2. Slow mode

From Fig. 6 it is clear that the slow decay mode displays a stretched nature, indicating a broad distribution of underlying decay time-scales, and this stretching is seen to increase with both scattering angle and concentration. From the fitting results, we find that β_s decreases both with increasing q and c (Fig. S14 (SI)), corresponding to the increasing stretching. Interestingly, the β_s values appear to fall into two groups for low and high concentrations, respectively. For $c \lesssim 0.065$ wt % ($c[\eta] \lesssim 1.0$), β_s spans the range ~ 0.7–1.0, and appears to level off towards ~ 0.7–0.8 for the highest q. For $\gtrsim 0.1$ wt % ($c[\eta] \gtrsim 1.5$), β_s is lower, spanning the range ~ 0.5–0.8; here, the existence of a high-q plateau is not so clear, but a weaker tendency to level off towards ~ 0.5–0.6 is observed. The c-dependent time-scale for the slow mode, $\langle\tau_s\rangle$, is shown in Fig. S11 (SI). The time-scale exhibits a significant c-dependence at all probed scattering angles, whereby $\langle\tau_s\rangle$ increases with c across the entire measured range. A comparison to Fig. 2 demonstrates that the c-dependence is similar to that of the specific viscosity and this result will be explored in more detail below.

The slow mode decay rates $\Gamma_s = \langle\tau_s\rangle^{-1}$ are shown renormalised by q^2, as $(\Gamma_s/q^2)/\langle\Gamma_s/q^2\rangle_q$ versus q in Fig. 7a, where $\langle\Gamma_s\rangle_q$ is the Γ_s value averaged over all q-values. For $q \gtrsim 10\ \mu m^{-1}$, the data for all concentrations increase with q, showing a clear departure from the plateau expected for diffusive scaling, for which $\Gamma_s \propto q^2$. In Fig. 7b, the data are

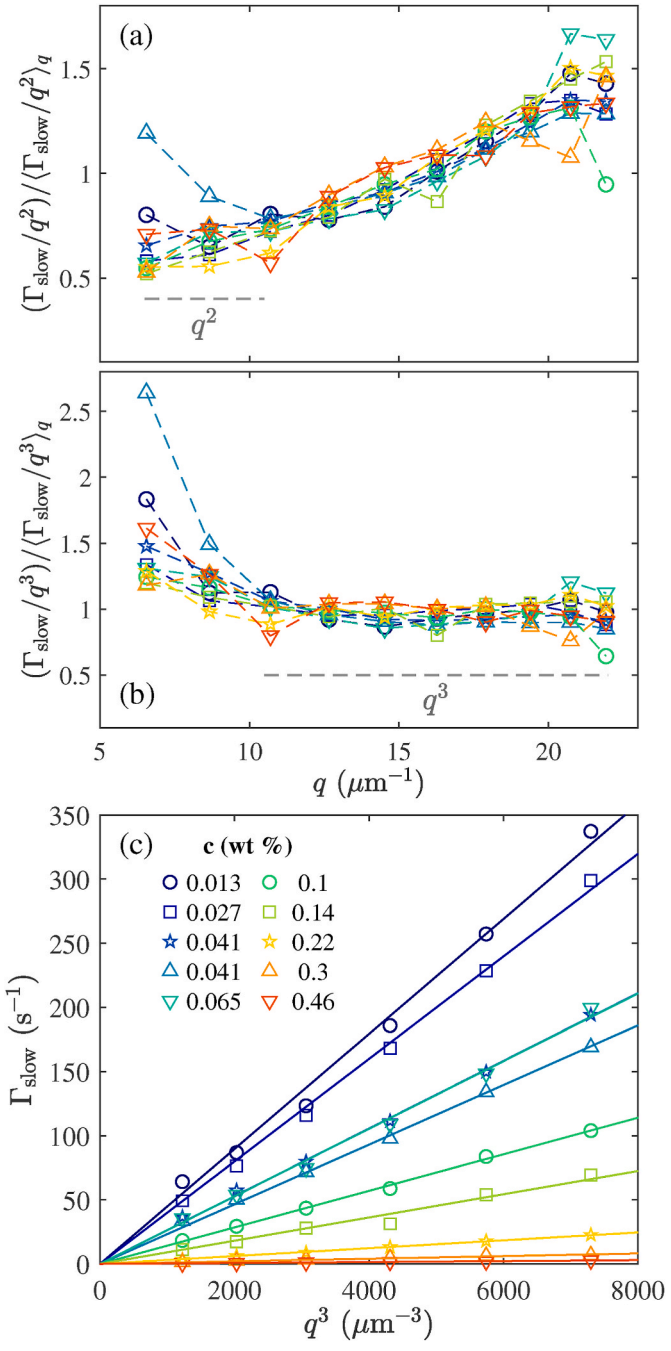

Fig. 7. The DLS slow mode decay rate: (a) divided by the square of the scattering wavevector and then re-normalised by the mean value for each concentration, plotted versus the scattering wavevector, q. The dashed horizontal line indicates $\Gamma_s \sim q^2$, as expected for diffusive behaviour. (b) Divided by the cube of the scattering wavevector, again re-normalised by the mean value for each c and plotted versus q. The dashed horizontal line indicates $\Gamma_s \sim q^3$, as expected for Zimm behaviour. (c) Plotted versus the cube of the scattering wavevector, q^3. The solid lines are linear fits fixed to pass through the origin.

instead re-normalised by q^3, and clearly show a plateau for $q \gtrsim 10\ \mu m^{-1}$. We note, however, that the q^2-scaled data do appear to flatten and approach a plateau for $q \lesssim 10\ \mu m^{-1}$. Thus, the slow mode decay rate transitions from approximately $\Gamma_s \sim q^2$ at the lowest scattering wavevectors to $\Gamma_s \sim q^3$, which is valid across most of the measured q range. This q^3-scaling is consistent with predictions for the Zimm model (Adam & Delsanti, 1977; Berne & Pecora, 2000; Doi & Edwards, 1986; Dubois-Violette & de Gennes, 1967; Sorlie & Pecora, 1988; Witte et al., 2019), indicating a transition with decreasing probed length-scale from simple diffusive behaviour to a probing of internal motions. We note that, for the Zimm model, the stretching parameter is predicted as $\beta_s = 2/3$ in the asymptotic high-q regime (Doi & Edwards, 1986), which is generally consistent with the β_s values found for the slow mode in the low concentration data (Fig. S14 (SI)).

In Fig. 7c, the slow mode decay rates are plotted versus q^3 (for 10 $\mu m^{-1} < q < 20\ \mu m^{-1}$, the $\Gamma_s \sim q^3$ regime) and linear fits are performed. The apparent viscosity η_{app} experienced by the polymer undergoing Zimm dynamics can be determined using the Zimm model (Eq. (9)), given the temperature and a value for the constant Λ. Thus, for a chosen Λ, the slope of each fit in Fig. 7c was used to calculate η_{app}, which was then converted to an apparent specific viscosity ($\eta_{sp,app} = (\eta_{app} - \eta_s)/\eta_s$). The resulting $\eta_{sp,app}(c)$ are shown in Fig. 8 for $\Lambda = 0.45$, for which the higher concentration data ($c[\eta] \gtrsim 1$) overlap with $\eta_{sp}(c)$. This empirical approach for choosing Λ was chosen since the theoretically predicted value varies somewhat depending on the approximations used, as discussed in Section 2. We note, however, that our chosen Λ is close to (~40% below) the values proposed by Adam and Delsanti (1977) and Richter et al. (2005). Within the dilute and lower semidilute unentangled regimes, $\eta_{sp,app}$ shows a reduced c-dependence, with enhanced values compared with η_{sp} as obtained from shear rheology. The two viscosities become closer as the concentration is increased, starting to overlap roughly halfway into the semidilute unentangled regime. Within the upper semidilute unentangled and semidilute entangled regimes the two viscosities show excellent agreement.

We suggest that the slow mode primarily arises from internal relaxations within LBG aggregates. This would explain why the corresponding apparent viscosities are relatively independent of c and larger

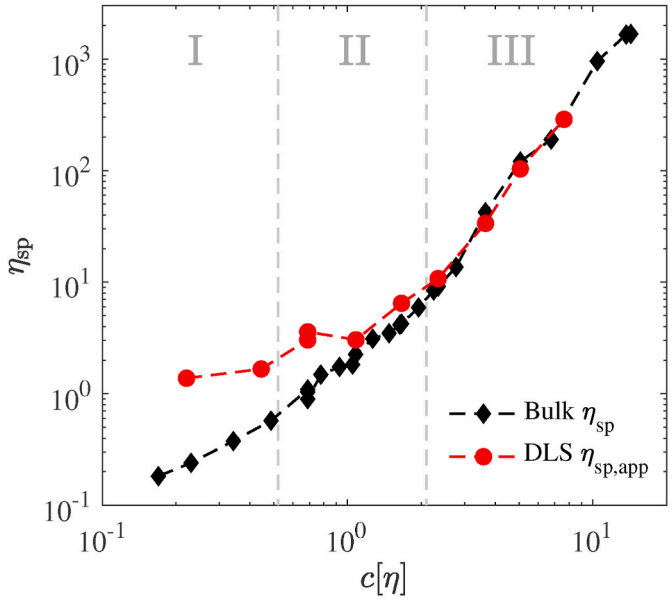

Fig. 8. Specific viscosity, η_{sp}, against reduced concentration, $c[\eta]$. Black data are determined from shear rheology measurements, as shown in Fig. 3. Red data are apparent specific viscosities, calculated using the Zimm relation (Eq. (9)) analysis of the slow mode DLS data, as described in the text. The concentration regimes identified from steady shear rheology are shown with grey dashed lines: I (dilute), II (semidilute unentangled), and III (semidilute entangled).

than the solution viscosity (which is mainly controlled by the dispersed polymer) in dilute solutions, where we expect little solute-solute interaction. As c is increased, however, interactions between dispersed LBG molecules and the aggregates cause the apparent viscosity and solution viscosity to approach each other, and they coincide for sufficiently high concentration.

Finally, apparent hydrodynamic radii were determined for the slow mode ($R_{h,s}$) by first calculating the average diffusion coefficient over the lowest two scattering wavevectors (q = 6.6 and 8.7 μm^{-1}), for which near-diffusive behaviour was observed. The Stokes-Einstein relation (Eq. (7)) was then used to calculate $R_{h,s}$ using these diffusion coefficients and the solution viscosity. $R_{h,s}$ was observed to decrease with concentration, from ~ 400 nm to ~ 200 nm as $c[\eta]$ varied from 0.2 to 7.6. Averaging over all concentrations, we found $\langle R_{h,s} \rangle_c = 290 \pm 100$ nm. This is significantly larger than one would expect for a single LBG molecule, further supporting the identification of the slow mode with supramolecular aggregates.

5. Conclusions

We have characterised the concentration-dependent structure and dynamics of locust bean gum (LBG) in aqueous solutions using a combination of static and dynamic light scattering, and steady state shear rheology. The weight-averaged molecular weight of LBG was determined from the intrinsic viscosity as $M_w = 1700 \pm 500$ kDa; the radius of gyration of the LBG polymer coil was estimated as $R_g = 92 \pm 9$ nm using the Flory-Fox relationship (assuming ideal chain conditions); and the mannose to galactose ratio (M:G) was determined as 3.4:1, using polarimetry. Steady shear rheology experiments were used to determine the concentration-dependent zero shear viscosity, which was found to split into three concentration scaling regimes, identified as the dilute, semidilute unentangled, and semidilute entangled regimes, respectively. Alternatively, the data could be adequately described either as a sum of two power laws, treating the intermediate concentrations as a continuous transition between the dilute and semidilute entangled regimes, or as a stretched exponential function, derived from hydrodynamic scaling theory (up to $c[\eta] = 4$, beyond which a power law description was required).

For the three-regime description, the regimes were described by $\eta_{sp} \sim c^{\zeta}$ with ζ = 1.03, 1.65, and 3.0, respectively, with boundaries defined by the overlap concentration c^* = 0.031 wt % ($c^*[\eta] = 0.52$, with $\eta_{sp}(c^*[\eta]) = 0.64$) and the entanglement concentration c^e = 0.13 wt % ($c^e[\eta] = 2.1$, with $\eta_{sp}(c^e[\eta]) = 6$). For the dilute and semidilute regimes, ζ is consistent with the predictions from scaling theory for neutral linear flexible polymers (Colby, 2010). For the entangled regime, however, our value is somewhat lower than the theoretically predicted value ($\zeta = 3.9$ for good solvent conditions). The specific viscosity values at c^* and c^e, as well as the width (c^e/c^*) of the semidilute unentangled regime, are consistent with previous results for neutral linear flexible polymers (Colby, 2010; Dumitriu, 2004). Our results are thus largely consistent with predictions for neutral flexible polymers and demonstrate that the solution viscosity mainly probes the well-dispersed polymer fraction.

The solution structure was investigated using a combination of static light scattering (SLS) and ultra-small-angle light scattering (USALS), where SLS probed the wavevector range q = 5.3–20.7 μm^{-1} and USALS the range 0.08–1.2 μm^{-1}. Within the SLS q-range, the excess Rayleigh ratio showed a power law behaviour $\Delta R(q) \propto c^e q^{-\gamma}$ for all concentrations, with average values of γ = 2.9 and ε = 0.77. No evidence was found for concentration-dependent structural transitions and the data instead demonstrates that the scattering is dominated by the internal structure of supramolecular aggregates whose properties change little with concentration. In future work, hydrodynamic separation techniques such as asymmetric flow field-flow fractionation may prove successful in separating the dispersed polymer from the aggregates, allowing for a more complete characterisation of these fractions, as has been achieved for other biopolymers (González-Espinosa, Sabagh,

Moldenhauer, Clarke, & Goycoolea, 2019). For lower q-values, USALS showed a plateau-like regime followed by a further increase in scattering intensity for $q \leq 0.2\ \mu m^{-1}$, where the behaviour is well-described as $\Delta R(q) \propto q^{\gamma_1}$, for all c, with an average value of $\gamma_1 = 2.4$. The SLS and USALS results together provide evidence for the existence of two separate populations of aggregated structures. We estimate the size of the smaller aggregates as $l \approx 670$ nm, consistent with the 600 nm pore-size of the filters used for sample preparation, and their molecular weight as 1.5 x 10^7 kDa—around 10^4 times larger than the polymer molecular weight. The lack of a roll-off for the lowest q probed with USALS, in turn, shows that the larger aggregates are characterised by a size greater than $\sim$ 14 μm, providing evidence for large supramolecular structures, at least 100 times greater than the expected R_g of a single LBG coil in dilute solution. We hypothesize that the unfiltered solutions contain aggregates larger than the pore size. Filtration, however, sets the aggregate size to roughly 600–700 nm and, in turn, these aggregates further associate into structures larger than $\sim$ 14 μm.

The solution dynamics were investigated using dynamic light scattering (DLS), showing a single 'slow' decay mode across the three concentration regimes, and an additional faster decay mode for the higher concentrations within the semidilute range; the data were thus fitted using either a single stretched exponential, or a sum of two stretched exponentials, as appropriate. Based on the amplitudes of the two decay modes, their respective contributions to the static scattering were determined. The main contribution to the SLS originates from polymer aggregates associated with the slow decay mode, whereas the fast mode contribution is very weak and becomes non-negligible only for the highest probed q-values; thus, the well-dispersed polymer fraction contributes only very weakly to the static scattering. We note that future complementary work using experimental techniques which can offer simultaneous insight into the dynamics of both the dispersed polymer and aggregates would be interesting; this might include pulsed field gradient nuclear magnetic resonance (NMR), for which the aggregate contribution should not dominate as in light scattering (Griffiths et al., 2002; Macdonald, Uemura, Dyke, & Zhu, 1996; Nilsson, Håkansson, Söderman, & Topgaard, 2007).

The fast decay mode in DLS is associated with the dispersed LBG phase. This decay mode is diffusive, characterised by a relatively fast time-scale and thus corresponding to short length-scale fluctuations (0.4–4 ms, with an apparent hydrodynamic radius of $R_{h,f} = 42$ nm using the solvent viscosity, or $\sim$ 2.7–0.3 nm using the solution viscosity, over the investigated concentration range), and observed within the semidilute entangled concentration regime. Based on these results, we assign the fast decay mode to cooperative diffusion and thus to fluctuations on the scale of the hydrodynamic correlation length, ξ_h, an assignment which is further supported by comparisons to the static correlation length (ξ_s) of LBG previously determined using small angle X-ray scattering and typical values of the cooperative diffusion coefficient determined for standard polymer systems.

In contrast to the fast decay mode, the slow mode decay rate follows a q^3 dependence over most of the q range. We interpret this as being due to internal Zimm relaxations within the LBG aggregates. Using Zimm theory, we determine the apparent specific viscosity ($\eta_{sp,app}$) from the slow mode decay rate, finding that this shows enhanced values and a weaker c-dependence compared to the solution viscosity within the dilute and lower semi-dilute unentangled regimes. The two viscosities approach as concentration is increased, and they overlap within the semi-dilute entangled regime. Within the dilute regime, the aggregates and dispersed LBG do not interact strongly, and the solution viscosity is mainly set by the dispersed polymer, explaining the behaviour. However, for higher concentrations, increased interactions between the dispersed polymer and aggregates lead to the convergence of the two viscosities.

In summary, we have combined light scattering with viscosity measurements to provide a comprehensive insight into both structure and dynamics of LBG in aqueous solution. To the best of our knowledge, this represents the first published dynamic light scattering investigation of aqueous LBG solutions. We demonstrate that a detailed determination of structure, dynamics, and viscosity can be achieved using only a relatively simple sample purification, which is important in order to ensure industrial relevance. This approach should also be valuable for other galactomannans, such as guar or tara gums, which have higher galactose content, and are thus more easily solubilised in water. Future work using a similar approach will investigate the influence of both temperature variation and the addition of co-solutes, providing fundamental as well as industrially relevant insight into the behaviour of LBG.

Author statement

All authors have read and approved the submitted manuscript and supplementary files in their final form.

Declaration of competing interest

The authors declare the following financial interests/personal relationships which may be considered as potential competing interests: Adam O'Connell reports financial support was provided by Unilever Plc. Co-author is Associate Editor of Food Hydrocolloids (F. M. Goycoolea).

Data availability

The data in this paper are available in the Leeds Data Repository (http://doi.org/10.5518/1266).

Acknowledgements

The authors acknowledge financial support from the Engineering and Physical Sciences Research Council (EPSRC) funded Centre for Doctoral Training in Soft Matter and Functional Interfaces (grant EP/L015536/1). We also thank the EPSRC for funding the photon correlation spectrometer used in the work on grant EP/J021156/1. J. M. is grateful for support from EPSRC on grant EP/K005073/1. This project has also received funding from the European Union's Horizon 2020 research and innovation programme under grant agreement No 731019 (EUSMI), for the USALS measurements. The authors thank Andrew Wilson and Martin Walko (School of Chemistry, University of Leeds) for their help with the polarimetry measurements.

Appendix A. Supplementary data

Supplementary data to this article can be found online at https://doi.org/10.1016/j.foodhyd.2022.108446.

References

Adam, M., & Delsanti, M. (1977). Dynamical properties of polymer solutions in good solvent by Rayleigh scattering experiments. *Macromolecules, 10*, 1229–1237. https://doi.org/10.1021/ma60060a014

Amis, E. J., & Han, C. C. (1982). Cooperative and self-diffusion of polymers in semidilute solutions by dynamic light scattering. *Polymer, 23*, 1403–1406. https://doi.org/10.1016/0032-3861(82)90236-1

Andrade, C. T., Azero, E. G., Luciano, L., & Gonçalves, M. P. (1999). Solution properties of the galactomannans extracted from the seeds of Caesalpinia pulcherrima and Cassia javanica: Comparison with locust bean gum. *International Journal of Biological Macromolecules, 26*, 181–185. https://doi.org/10.1016/S0141-8130(99)00075-6

Barak, S., & Mudgil, D. (2014). Locust bean gum: Processing, properties and food applications—a review. *International Journal of Biological Macromolecules, 66*, 74–80. https://doi.org/10.1016/j.ijbiomac.2014.02.017

Berne, B. J., & Pecora, R. (2000). *Dynamic light scattering with applications to Chemistry, biology, and physics*. Mineola, New York: Dover.

Berry, G. C., & Cotts, P. M. (1999). Static and dynamic light scattering. In R. A. Pethrick, & J. V. Dawkins (Eds.), *Modern techniques for polymer characterisation*. London: John Wiley & Sons, Ltd.

Bhatia, S. R. (2005). Ultra-small-angle scattering studies of complex fluids. *Current Opinion in Colloid & Interface Science, 9*, 404–411. https://doi.org/10.1016/j.cocis.2004.10.001

Borsali, R., & Pecora, R. (2008). *Soft matter characterization*. New York: Springer.

Brown, W., & Nicolai, T. (1990). Static and dynamic behavior of semidilute polymer solutions. *Colloid & Polymer Science, 268*, 977–990. https://doi.org/10.1007/BF01410586

Brown, W., & Zhou, P. (1991). Solution properties of polyisobutylene investigated by using dynamic and static light scattering and pulsed field gradient NMR. *Macromolecules, 24*, 5151–5157. https://doi.org/10.1021/ma00018a020

Burchard, W., & Eisele, M. (1984). Cooperative motion and self-diffusion in dilute and semidilute poly-vinylpyrrolidone solutions. *Pure and Applied Chemistry, 56*, 1379–1390. https://doi.org/10.1351/pac198456101379

Burchard, W., & Richtering, W. (1989). Dynamic light scattering from polymer solutions. In *Relaxation in polymers* (pp. 151–163). Darmstadt: Steinkopff.

Cerqueira, M. A., Bourbon, A. I., Pinheiro, A. C., Martins, J. T., Souza, B. W. S., Teixeira, J. A., et al. (2011). Galactomannans use in the development of edible films/coatings for food applications. *Trends in Food Science & Technology, 22*, 662–671. https://doi.org/10.1016/j.tifs.2011.07.002

Cipelletti, L., & Weitz, D. A. (1999). Ultralow-angle dynamic light scattering with a charge coupled device camera based multispeckle, multitau correlator. *Review of Scientific Instruments, 70*, 3214–3221. https://doi.org/10.1063/1.1149894

Colby, R. H. (2010). Structure and linear viscoelasticity of flexible polymer solutions: Comparison of polyelectrolyte and neutral polymer solutions. *Rheologica Acta, 49*, 425–442. https://doi.org/10.1007/s00397-009-0413-5

Cosgrove, T., & Sutherland, J. M. (1983). Self and mutual diffusion measurements in dilute and semi-dilute polystyrene solutions. *Polymer, 24*, 534–536. https://doi.org/10.1016/0032-3861(83)90100-3

Daas, P. J., Schols, H. A., & De Jongh, H. H. (2000). On the galactosyl distribution of commercial galactomannans. *Carbohydrate Research, 329*, 609–619. https://doi.org/10.1016/S0008-6215(00)00209-3

Dakia, P. A., Blecker, C., Robert, C., Wathelet, B., & Paquot, M. (2008). Composition and physicochemical properties of locust bean gum extracted from whole seeds by acid or water dehulling pre-treatment. *Food Hydrocolloids, 22*, 807–818. https://doi.org/10.1016/j.foodhyd.2007.03.007

Dea, I. C., Clark, A. H., & McCleary, B. V. (1986). Effect of the molecular fine structure of galactomannans on their interaction properties — the role of unsubstituted sides. *Food Hydrocolloids, 1*, 129–140. https://doi.org/10.1016/S0268-005X(86)80015-7

Dea, I. C., Morris, E. R., Rees, D. A., Welsh, E., Barnes, H. A., & Price, J. (1977). Associations of like and unlike polysaccharides: Mechanism and specificity in galactomannans, interacting bacterial polysaccharides, and related systems. *Carbohydrate Research, 57*, 249–272. https://doi.org/10.1016/S0008-6215(00)81935-7

Doi, M., & Edwards, S. F. (1986). *The theory of polymer dynamics*. Oxford: Oxford University Press.

Doublier, J. L., & Launary, B. (1981). Rheology of Galactomannan solutions: Comparative study of guar gum and locust bean gum. *Journal of Texture Studies, 12*, 151–172.

Doyle, J. P., Lyons, G., & Morris, E. R. (2009). New proposals on "hyperentanglement" of galactomannans: Solution viscosity of fenugreek gum under neutral and alkaline conditions. *Food Hydrocolloids, 23*, 1501–1510. https://doi.org/10.1016/j.foodhyd.2008.09.007

Dubois-Violette, E., & de Gennes, P. G. (1967). Quasi-elastic scattering by dilute, ideal, polymer solutions: II. Effects of hydrodynamic interactions. *Physics, 3*, 181–198. https://doi.org/10.1103/physicsphysiquefizika.3.181

Dumitriu, S. (2004). *Polysaccharides*. New York: Marcel Dekker.

Ewoldt, R. H., Johnston, M. T., & Caretta, L. M. (2015). Experimental challenges of shear rheology: How to avoid bad data. In *Complex fluids in biological systems* (pp. 207–241). Springer. https://doi.org/10.1007/978-1-4939-2065-5_6.

Ferri, F. (1997). Use of a charge coupled device camera for low-angle elastic light scattering. *Review of Scientific Instruments, 68*, 2265–2274. https://doi.org/10.1063/1.1148135

Gaisford, S. E., Harding, S. E., Mitchell, J. R., & Bradley, T. D. (1986). A comparison between the hot and cold water soluble fractions of two locust bean gum samples. *Carbohydrate Polymers, 6*, 423–442. https://doi.org/10.1016/0144-8617(86)90002-0

Ganter, J. L., Milas, M., Corrêa, J. B., Reicher, F., & Rinaudo, M. (1992). Study of solution properties of galactomannan from the seeds of Mimosa scabrella. *Carbohydrate Polymers, 17*, 171–175. https://doi.org/10.1016/0144-8617(92)90001-7

Garnier, C., Schorsch, C., & Doublier, J. L. (1995). Phase separation in dextran/locust bean gum mixtures. *Carbohydrate Polymers, 28*, 313–317. https://doi.org/10.1016/0144-8617(95)00090-9

de Gennes, P. G. (1979). *Scaling concepts in polymer physics*. London: Cornell University Press.

Gillet, S., Aguedo, M., Petrut, R., Olive, G., Anastas, P., Blecker, C., et al. (2017). Structure impact of two galactomannan fractions on their viscosity properties in dilute solution, unperturbed state and gel state. *International Journal of Biological Macromolecules, 96*, 550–559. https://doi.org/10.1016/j.ijbiomac.2016.12.057

Gittings, M. R., Cipelletti, L., Trappe, V., Weitz, D. A., In, M., & Marques, C. (2000). Structure of guar in solutions of H2O and D2O: An ultra-small-angle light-scattering study. *Journal of Physical Chemistry B, 104*, 4381–4386. https://doi.org/10.1021/jp9943833

Goff, H. D., Ferdinando, D., & Schorsch, C. (1999). Fluorescence microscopy to study galactomannan structure in frozen sucrose and milk protein solutions. *Food Hydrocolloids, 13*, 353–362. https://doi.org/10.1016/S0268-005X(99)00017-X

González-Espinosa, Y., Sabagh, B., Moldenhauer, E., Clarke, P., & Goycoolea, F. M. (2019). Characterisation of chitosan molecular weight distribution by multi-detection asymmetric flow-field flow fractionation (AF4) and SEC. *International Journal of Biological Macromolecules, 136*, 911–919. https://doi.org/10.1016/j.ijbiomac.2019.06.122

Goycoolea, F. M., Morris, E. R., & Gidley, M. J. (1995). Viscosity of galactomannans at alkaline and neutral pH: Evidence of 'hyperentanglement' in solution. *Carbohydrate Polymers, 27*, 69–71. https://doi.org/10.1016/0144-8617(95)00030-B

Grenha, A., & Dionísio, M. (2012). Locust bean gum: Exploring its potential for biopharmaceutical applications. *Journal of Pharmacy and BioAllied Sciences, 4*, 175. https://doi.org/10.4103/0975-7406.99013

Griffiths, P. C., Cheung, A. Y., Davies, J. A., Paul, A., Tipples, C. N., & Winnington, A. L. (2002). Probing interactions within complex colloidal systems using PGSE-NMR. *Magnetic Resonance in Chemistry, 40*, 40–50. https://doi.org/10.1002/mrc.1131

Hammouda, B., Ho, D. L., & Kline, S. (2004). Insight into clustering in poly(ethylene oxide) solutions. *Macromolecules, 37*, 6932–6937. https://doi.org/10.1021/ma049623d

Han, C. C., & Akcasu, A. Z. (1981). Dynamic light scattering of dilute polymer solutions in the nonasymptotic q region. *Macromolecules, 14*, 1080–1084. https://doi.org/10.1021/ma50005a037

Hellebois, T., Soukoulis, C., Xu, X., Hausman, J. F., Shaplov, A., Taoukis, P. S., et al. (2021). Structure conformational and rheological characterisation of alfalfa seed (Medicago sativa L.) galactomannan. *Carbohydrate Polymers, 256*. https://doi.org/10.1016/j.carbpol.2020.117394

Ioan, C. E., Aberle, T., & Burchard, W. (2001). Light scattering and viscosity behavior of dextran in semidilute solution. *Macromolecules, 34*, 326–336. https://doi.org/10.1021/ma992060z

Ioannidou, K., Krakowiak, K. J., Bauchy, M., Hoover, C. G., Masoero, E., Yip, S., et al. (2016). Mesoscale texture of cement hydrates. *Proceedings of the National Academy of Sciences of the United States of America, 113*, 2029–2034. https://doi.org/10.1073/pnas.1520487113

Kanematsu, T., Sato, T., Imai, Y., Ute, K., & Kitayama, T. (2005). Mutual- and self-diffusion coefficients of a semiflexible polymer in solution. *Polymer Journal, 37*, 65–73. https://doi.org/10.1295/polymj.37.65

Launay, B., Cuvelier, G., & Martinez-Reyes, S. (1997). Viscosity of locust bean, guar and xanthan gum solutions in the Newtonian domain: A critical examination of the log (ηsp)o-log c[η]o master curves. *Carbohydrate Polymers, 34*, 385–395. https://doi.org/10.1016/S0144-8617(97)00104-5

Li, J., Ngai, T., & Wu, C. (2010). The slow relaxation mode: From solutions to gel networks. *Polymer Journal, 42*, 609–625. https://doi.org/10.1038/pj.2010.59

Liu, B., Huang, Y., Wang, J., Li, Z., Yang, G., Jin, S., et al. (2021). Highly conductive locust bean gum bio-electrolyte for superior long-life quasi-solid-state zinc-ion batteries. *RSC Advances, 11*, 24862–24871. https://doi.org/10.1039/d1ra04294g

Lopes da Silva, J. A., & Goncalves, M. P. (1990). Studies on a purification method for locust bean gum by precipitation with isopropanol. *Food Hydrocolloids, 4*, 277–287. https://doi.org/10.1016/S0268-005X(09)80204-X

Macdonald, P. M., Uemura, Y., Dyke, L., & Zhu, X. (1996). Self-Diffusion coefficients of associating polymers from pulsed-gradient spin-echo nuclear magnetic resonance spectroscopy. *Advances in Chemistry Series, 248*, 391–393. https://doi.org/10.1021/ba-1996-0248.ch020

Maiti, S., Dey, P., Banik, A., Sa, B., Ray, S., & Kaity, S. (2010). Tailoring of locust bean gum and development of hydrogel beads for controlled oral delivery of glipizide. *Drug Delivery, 17*, 288–300. https://doi.org/10.3109/10717541003706265

McCleary, B. V., Clark, A. H., Dea, I. C., & Rees, D. A. (1985). The fine structures of carob and guar galactomannans. *Carbohydrate Research, 139*, 237–260. https://doi.org/10.1016/0008-6215(85)90024-2

Morris, E. R., Cutler, A. N., Ross-Murphy, S. B., Rees, D. A., & Price, J. (1981). Concentration and shear rate dependence of viscosity in random coil polysaccharide solutions. *Carbohydrate Polymers, 1*, 5–21. https://doi.org/10.1016/0144-8617(81)90011-4

Nicolai, T., & Brown, W. (1996). Cooperative diffusion of concentrated polymer solutions: A static and dynamic light scattering study of polystyrene in DOP. *Macromolecules, 29*, 1698–1704. https://doi.org/10.1021/ma946430p

Nilsson, M., Håkansson, B., Söderman, O., & Topgaard, D. (2007). Influence of polydispersity on the micellization of triblock copolymers investigated by pulsed field gradient nuclear magnetic resonance. *Macromolecules, 40*, 8250–8258. https://doi.org/10.1021/ma071302p

Noble, O., Perez, S., Rochas, C., & Taravel, F. (1986). Optical rotation of branched polysaccharides - the galactomannan case. *Polymer Bulletin, 16*, 175–180. https://doi.org/10.1007/BF00955488

Nyström, B., Walderhaug, H., & Hansen, F. K. (1993). Dynamic crossover effects observed in solutions of a hydrophobically associating water-soluble polymer. *Journal of Physical Chemistry, 97*, 7743–7752. https://doi.org/10.1021/j100131a052

Parafati, L., Vitale, A., Restuccia, C., & Cirvilleri, G. (2016). The effect of locust bean gum (LBG)-based edible coatings carrying biocontrol yeasts against Penicillium digitatum and Penicillium italicum causal agents of postharvest decay of Mandarin fruit. *Food Microbiology, 58*, 87–94. https://doi.org/10.1016/j.fm.2016.03.014

Patmore, J. V., Goff, H. D., & Fernandes, S. (2003). Cryo-gelation of galactomannans in ice cream model systems. *Food Hydrocolloids, 17*, 161–169. https://doi.org/10.1016/S0268-005X(02)00048-6

Pegg, A. (2012). The application of natural hydrocolloids to foods and beverages. In *Natural food additives, ingredients and flavourings* (pp. 175–196). Elsevier. https://doi.org/10.1533/9780857095725.1.175.

Perestrelo, A. R., Grenha, A., Rosa Da Costa, A. M., & António Belo, J. (2014). Locust bean gum as an alternative polymeric coating for embryonic stem cell culture. *Materials Science and Engineering: C, 40*, 336–344. https://doi.org/10.1016/j.msec.2014.04.022

Petkowicz, C. L., Reicher, F., & Mazeau, K. (1998). Conformational analysis of galactomannans: From oligomeric segments to polymeric chains. *Carbohydrate Polymers, 37*, 25–39. https://doi.org/10.1016/S0144-8617(98)00051-4

Phillies, G. D. (1995). Hydrodynamic scaling of viscosity and viscoelasticity of polymer solutions, including chain architecture and solvent quality effects. *Macromolecules, 28*, 8198–8208. https://doi.org/10.1021/ma00128a033

Phillies, G. D. J. (2011). *Phenomenology of polymer solution dynamics*. Cambridge: Cambridge University Press.

Phillies, G. D., & Quinlan, C. A. (1995). Analytic structure of the solutionlike-meltlike transition in polymer dynamics. *Macromolecules, 28*, 160–164. https://doi.org/10.1021/ma00105a021

Picout, D. R., & Ross-Murphy, S. B. (2007). On the Mark–Houwink parameters for galactomannans. *Carbohydrate Polymers, 70*, 145–148. https://doi.org/10.1016/j.carbpol.2007.03.010

Picout, D. R., Ross-Murphy, S. B., Errington, N., & Harding, S. E. (2001). Pressure cell assisted solution characterization of polysaccharides. 1. *Guar gum. Biomacromolecules, 2*, 1301–1309. https://doi.org/10.1021/bm010118n

Picout, D. R., Ross-Murphy, S. B., Jumel, K., & Harding, S. E. (2002). Pressure cell assisted solution characterization of polysaccharides. 2. Locust bean gum and tara gum. *Biomacromolecules, 3*, 761–767. https://doi.org/10.1021/bm025517c

Pollard, M. A., & Fischer, P. (2014). Semi-dilute galactomannan solutions: Observations on viscosity scaling behavior of guar gum. *Journal of Physics: Condensed Matter, 26*, Article 464107. https://doi.org/10.1088/0953-8984/26/46/464107

Potier, M., Tea, L., Benyahia, L., Nicolai, T., & Renou, F. (2020). Viscosity of aqueous polysaccharide solutions and selected homogeneous binary mixtures. *Macromolecules, 53*, 10514–10525. https://doi.org/10.1021/acs.macromol.0c02157

Richardson, P. H., & Norton, I. T. (1998). Gelation behavior of concentrated locust bean gum solutions. *Macromolecules, 31*, 1575–1583. https://doi.org/10.1021/ma970550q

Richardson, P. H., Willmer, J., & Foster, T. J. (1998). Dilute solution properties of guar and locust bean gum in sucrose solutions. *Food Hydrocolloids, 12*. https://doi.org/10.1016/S0268-005X(98)00025-3

Richter, S., Boyko, V., Matzker, R., & Schröter, K. (2004). Gelation studies: Comparison of the critical exponents obtained by dynamic light scattering and rheology, 2a. A thermoreversible gelling system: Mixtures of xanthan gum and locust-bean gum. *Macromolecular Rapid Communications, 25*, 1504–1509. https://doi.org/10.1002/marc.200400214

Richter, D., Monkenbusch, M., Arbe, A., & Colmenero, J. (2005). *Neutron spin echo in polymer systems*. Berlin: Springer. https://doi.org/10.1007/978-3-642-27154-0

Rubinstein, M., & Colby, R. H. (2003). *Polymer physics*. Oxford: Oxford University Press.

Saha, D., & Bhattacharya, S. (2010). Hydrocolloids as thickening and gelling agents in food: A critical review. *Journal of Food Science & Technology, 47*, 587–597. https://doi.org/10.1007/s13197-010-0162-6. arXiv:arXiv:1011.1669v3.

Schärtl, W. (2007). *Light scattering from polymer solutions and nanoparticle dispersions*. Berlin Heidelberg: Springer.

Schorsch, C., Jones, M. G., & Norton, I. T. (1999). Thermodynamic incompatibility and microstructure of milk protein/locust bean gum/sucrose systems. *Food Hydrocolloids, 13*, 89–99. https://doi.org/10.1016/S0268-005X(98)00074-5

Sébastien, G., Christophe, B., Mario, A., Pascal, L., Michel, P., & Aurore, R. (2014). Impact of purification and fractionation process on the chemical structure and physical properties of locust bean gum. *Carbohydrate Polymers, 108*, 159–168. https://doi.org/10.1016/j.carbpol.2014.02.092

Sittikijyothin, W., Torres, D., & Gonçalves, M. (2005). Modelling the rheological behaviour of galactomannan aqueous solutions. *Carbohydrate Polymers, 59*, 339–350. https://doi.org/10.1016/J.CARBPOL.2004.10.005

Sorlie, S. S., & Pecora, R. (1988). A dynamic light scattering study of a 2311 base pair DNA restriction fragment. *Macromolecules, 21*, 1437–1449. https://doi.org/10.1021/ma00183a039

Tagad, C. K., Rajdeo, K. S., Kulkarni, A., More, P., Aiyer, R. C., & Sabharwal, S. (2014). Green synthesis of polysaccharide stabilized gold nanoparticles: Chemo catalytic and room temperature operable vapor sensing application. *RSC Advances, 4*, 24014–24019. https://doi.org/10.1039/c4ra02972k

Tanaka, R., Hatakeyama, T., & Hatakeyama, H. (1998a). Formation of locust bean gum hydrogel by freezing-thawing. *Polymer International, 45*, 118–126. https://doi.org/10.1002/(SICI)1097-0126 (199801)45:1¡118::AID-PI908¿3.0.CO;2-T.

Tanaka, R., Hatakeyama, T., & Hatakeyama, H. (1998b). Interaction between polymer molecules in locust bean gum-water systems during cooling and freezing processes. In *Gums and stabilisers for the food industry 9* (pp. 43–47). Elsevier. https://doi.org/10.1533/9781845698362.1.43.

Teixeira, J. (1986). Experimental methods for studying fractal aggregates. In *On growth and form: Fractal and non-fractal patters in physics* (pp. 145–162). Dordrecht: Martinus Nijhoff Publishers.

Turquois, T., Rochas, C., Taravel, F., Doublier, J. L., & Axelos, M. (1995). Small-angle x-ray scattering of κ-carrageenan based systems: Sols, gels, and blends with carob galactomannan. *Biopolymers, 36*, 559–567. https://doi.org/10.1002/bip.360360502

Uematsu, T., Svanberg, C., & Jacobsson, P. (2005). A unified picture of static and dynamic length scales in polymer solutions. *Macromolecules, 38*, 6227–6230. https://doi.org/10.1021/ma050478t

Uematsu, T., Svanberg, C., Nydén, M., & Jacobsson, P. (2003). Power laws in polymer solution dynamics. *Physical Review A, 68*, 1–8. https://doi.org/10.1103/PhysRevE.68.051803

Ventura, M. G., Paninho, A. I., Nunes, A. V., Fonseca, I. M., & Branco, L. C. (2015). Biocompatible locust bean gum mesoporous matrices prepared by ionic liquids and a scCO2 sustainable system. *RSC Advances, 5*, 107700–107706. https://doi.org/10.1039/c5ra17314k

Vlassopoulos, D., & Schowalter, W. R. (1994). Steady viscometric properties and characterization of dilute drag-reducing polymer solutions. *Journal of Rheology, 38*, 1427–1446. https://doi.org/10.1122/1.550605

Wientjes, R. H., Duits, M. H., Jongschaap, R. J., & Mellema, J. (2000). Linear rheology of guar gum solutions. *Macromolecules, 33*, 9594–9605. https://doi.org/10.1021/ma001065p

Witte, J., Kyrey, T., Lutzki, J., Dahl, A. M., Houston, J., Radulescu, A., et al. (2019). A comparison of the network structure and inner dynamics of homogeneously and heterogeneously crosslinked PNIPAM microgels with high crosslinker content. *Soft Matter, 15*, 1053–1064. https://doi.org/10.1039/c8sm02141d

Wu, H. (2010). Correlations between the Rayleigh ratio and the wavelength for toluene and benzene. *Chemical Physics, 367*, 44–47. https://doi.org/10.1016/j.chemphys.2009.10.019

Yuan, G., Wang, X., Han, C. C., & Wu, C. (2006). Reexamination of slow dynamics in semidilute solutions: Temperature and salt effects on semidilute poly(N-isopropylacrylamide) aqueous solutions. *Macromolecules, 39*, 6207–6209. https://doi.org/10.1021/ma061059e

Zettl, U., Hoffmann, S. T., Koberling, F., Krausen, G., Enderlein, J., Harnau, L., et al. (2009). Self-diffusion and cooperative diffusion in semidilute polymer solutions as measured by fluorescence correlation spectroscopy. *Macromolecules, 42*, 9537–9547. https://doi.org/10.1021/ma901404g. arXiv:1002.0926.